Chemistry–A European Journal

Supporting Information

Sugar-Bridged Fullerene Dumbbells and Their Interaction with the [10]Cycloparaphenylene Nanoring

Jovana Jakšić, Iris Solymosi, Andreas Hirsch, M. Eugenia Pérez-Ojeda,* Aleksandra Mitrović,* and Veselin Maslak*

Table of Contents

All reagents and solvents were purchased from commercial sources, and used without further purifications. All solvents were dried prior to use according to standard literature protocols. Flash chromatography was performed on SiO_2 (0.018–0.032 mm). Thin-layer chromatography (TLC) was carried out on precoated silica gel 60 F_{254} plates (Merck). IR spectra (ATR) were recorded on a Perkin-Elmer-FT-IR 1725X spectrophotometer; v values are given in cm^{-1}.

^{1}H and ^{13}C NMR spectra were recorded on a Bruker Ultrashield Avance III (1H at 500 MHz, 13C at 125 MHz) and Bruker Ascend 400 (400 MHz) (^{1}H at 400 MHz, ^{13}C at 100 MHz) spectrometers using CS_2/$CDCl_3$ or $CDCl_3$ as solvents and TMS as an internal standard. Chemical shifts (δ) are expressed in parts-per million (ppm) and coupling constants (J) in Hz. The following abbreviations were used for signal multiplicities (s = singlet, d = doublet, t = triplet, q = quartet, quin = quintet, sex = sextet, m = multiplet, etc.). Homonuclear 2D (DQF-COSY and NOESY) and heteronuclear 2D 1H-13C spectra (HSQC, HMBC) were recorded with the usual settings.

UV spectra were recorded with a COLO NOVEL4S UV-vis spectrophotometer.

The high-resolution MS spectra were taken with Agilent 6210 LC ESI-MS TOF spectrometer.

Cyclic Voltammetry and Linear sweep voltammetry measurements were recorded with METROHM Autolab PGSTAT128N, using Glassy carbon electrode as a working electrode, Ag/AgCl as a reference electrode and Platinum sheet electrode as a counter electrode. Tetrabutylammonium hexafluorophosphate (0.01 M) (98%, Sigma- Aldrich) was used as a supporting electrolyte.

Thermogravimetric analysis (TGA) of the products were carried out using a PerkinElmer Pyris 1 TGA instrument under constant nitrogen flow (20 mL/min), with a isotherm at 25 °C for one minute and a subsequent heating rate of 10 K/min.

Optimization of the reaction conditions for obtaining furan-fused fullerenes

Table S1. Reaction conditions for obtaining **10$_{IS}$**

Entry[a]	**9** (eq.)	DBU (eq.)	TEMPO (eq.)	Yield[b] (%)
1	0.5	20	2	0
2	1	20	2	7
3	1.5	20	2	17
4	2	20	2	19
5	3	20	2	24
6	3	40	4	21

[a] **6** (0.0067 mmol), 15 mL toluene, Ar. [b] Isolated yield was calculated in relation to the amount of added bis-β-keto ester **6**.

Experimental protocols

Synthesis of compound 4
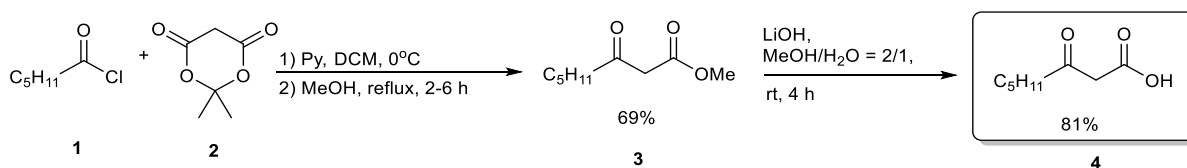
Scheme S1. Synthesis of 3-oxooctanoic acid **4**.

Anhydrous DCM (50 mL) was added to Meldrum's acid **2** (5.35 g, 40 mmol, 1 eq.) at 0°C under argon atmosphere. Pyridine (6 mL, 70 mmol, 2 eq.) was added dropwise at 0°C over 20 min. Hexanoyl chloride **1** (5.2 mL, 40 mmol, 1 eq.) was added at 0°C and the mixture was left to stir for 2 h at 0°C and allowed to warm to room temperature with stirring over 1 h. The reaction mixture was diluted with 40 mL DCM and poured into 50 mL of an ice/HCl aq (2M) mixture. The resultant mixture was stirred for 10 min, the aqueous and organic phases were separated and the organic phase was washed with 80 mL HCl (2M) followed by saturated brine (80 mL). The organic layer was dried over anhydrous Na$_2$SO$_4$ and the solvent removed under reduced pressure. The resultant crude product material was dissolved in 140 mL methanol and heated to reflux under argon atmosphere with stirring for 5 h. The solvent was removed under reduced pressure and the resultant product material purified by column chromatography with petroleum ether/ethyl acetate (8: 2 v/v) to give pure methyl 3-oxooctanoate **3** (4.76 g, 69%). The spectra obtained were in accordance with those reported in literature. [23a]

Lithium hydroxide (834 mg, 34.8 mmol, 4 eq.) was added to the solution of methyl 3-oxooctanoate **3** (1.5 g, 8.7 mmol, 1 eq.) in 90 mL mixture of solvents methanol/water (2/1). The reaction mixture was stirred for 24 hours at room temperature, then solvents were evaporated under vacuum. The mixture was acidified to pH 2 using HCl, and the resulting solution was washed with ethyl acetate (3 × 30 mL) followed by washing with brine and drying over anhydrous Na$_2$SO$_4$. The solvent was evaporated under reduced pressure, and desired 3-oxooctanoic acid **4** (1.11 g, 81%) was obtained. The spectra obtained were in accordance with those reported in literature. [23b]

Synthesis of compounds 6, 8

N,N′-dicyclohexylcarbodiimide (DCC) (1.18 g, 5.70 mmol, 3 eq.) and 4-dimethylaminopyridine (DMAP) (61 mg, 0.5 mmol) were added to the solution of 3-oxooctanoic acid **4** (600 mg, 3.80 mmol, 2 eq.) in 40 mL DCM and the mixture was left to stir for 5 min at 0°C. The appropriate isohexide (1,4:3,6-dianhydrohexitol) **5** or **7** (278 mg, 1.90 mmol, 1 eq.) was added to the reaction mixture and stirring was continued for 24 h at room temperature. After the reaction was completed, the solvent was evaporated by increasing the temperature under reduced pressure. The residue was dissolved in 40 mL of ethyl acetate and filtered under reduced pressure to remove the dicyclohexylurea (DCU). The filtrate was concentrated and the crude product was chromatographed on a silica gel column with petroleum ether/ethyl acetate (6: 4 v/v) to give pure bis β-keto ester-isohexide derivate **6** or **8**.

(3*R*,3a*R*,6*S*,6a*R*)-hexahydrofuro[3,2-b]furan-3,6-diyl bis(3-oxooctanoate) (6): 486 mg, 60%, white crystalline solid; ^{1}H NMR (500 MHz, CDCl$_3$): δ 11.86 (bs, 1H enol-OH), 11.85 (bs, 1H enol-OH), 5.26 (d, *J* = 2.9 Hz, **C2**-1H), 5.22 – 5.16 (m, **C5**-1H), 5.06 (s, 1H enol), 4.98 (s, 1H enol), 4.87 – 4.81 (m, **C4**-1H), 4.54 (d, *J* = 4.6 Hz, 1H enol), 4.52 (d, *J* = 4.5 Hz, **C3**-1H), 4.02 – 3.92 (m, **C1**-2H, **C6**-1H), 3.83 (dd, *J$_1$* = 10.0 Hz, *J$_2$* = 5.1 Hz, **C6**-1H), 3.49 (s, 2H), 3.45 (s, 2H), 2.55 (t, *J* = 7.4 Hz, 2H), 2.49 (t, *J* = 7.4 Hz, 2H), 2.22 – 2.17 (m, 4H enol), 1.63 – 1.55 (m, 4H), 1.35 – 1.24 (m, 8H), 0.89 (t, *J* = 7.0 Hz, 6H) ppm; ^{13}C NMR (125 MHz, CDCl$_3$): δ 202.5 (keto), 202.4 (keto) and 180.6 (enol), 180.4 (enol), 172.0 (enol), 171.8 (enol) and 166.7 (keto), 166.5 (keto), 88.6 and 88.4 (enol), 86.3 (enol) and 86.0 (keto), 81.2 (enol) and 80.8 (keto), 79.0 (enol) and 78.8 (keto), 74.9 (keto) and 73.6 (enol), 73.5 and 73.4 (enol) and 73.3 (keto), 70.5 (keto) and 70.4 (enol), 49.1 (keto), 43.3 and 43.1 (keto) and 35.3 (enol), 31.4 (enol) and 31.31 and 31.30 (keto), 26.04 and 26.02 (enol) and 23.3 (keto), 22.53 (keto) and 22.49 (enol), 14.0 ppm. IR (ATR): ν 3623, 2957, 2933, 2871, 1749, 1717, 1651, 1316, 1232, 1156, 1095 cm^{-1}; m.p. 32.8-34.0ºC; $[\alpha]_{589}^{20}$ = 59º; Elem. Anal. (calculated): C 61.95, H 8.04 %; Elem. Anal. (found): C 61.78, H 7.82 %.

(3*R*,3a*R*,6*R*,6a*R*)-hexahydrofuro[3,2-b]furan-3,6-diyl bis(3-oxooctanoate) (8): 503 mg, 62%, white crystalline solid; ^{1}H NMR (500 MHz, CDCl$_3$): δ 11.82 (bs, 1H enol-OH), 11.81 (bs, 1H enol-OH), 5.19 – 5.09 (m, **C5**-1H, **C2**-1H), 5.07 (s, 2H enol), 4.73 – 4.66 (m, **C4**-1H, **C3**-1H), 4.07 – 4.00 (m, **C6**-1H, **C1**-1H), 3.83 (dd, *J$_1$* = 9.5 Hz, *J$_2$* = 6.3 Hz, **C6**-1H, **C1**-1H enol), 3.77 (dd, *J$_1$* = 9.4 Hz, *J$_2$* = 6.9 Hz, **C6**-1H, **C1**-1H), 3.49 (s, 4H), 2.54 (t, *J* = 7.4 Hz, 4H), 2.19 (t, *J* = 7.6 Hz, 4H enol), 1.62 – 1.52 (m, 4H), 1.34 – 1.22 (m, 8H), 0.87 (t, *J* = 7.0 Hz, 6H) ppm; ^{13}C NMR (125 MHz, CDCl$_3$): δ 202.4 (keto), 180.43 and 180.36 (enol), 172.0 and 171.9 (enol), 166.7 (keto), 88.40 and 88.37 (enol), 80.8 (enol) and 80.4 (keto), 74.6 (enol) and 74.5 (keto), 73.2 (enol), 70.6 (enol) and 70.4 (keto), 49.0 (keto), 43.0 (keto) and 35.2 (enol), 31.30 (enol) and 31.26 (keto), 26.0 (enol) and 23.2 (keto), 22.49 (keto) and 22.46 (enol), 14.0 ppm; IR (ATR): ν 2956, 2932, 2869, 1747, 1716, 1650, 1316, 1233, 1154, 1057 cm^{-1}; $[\alpha]_{589}^{20}$ = 178º; Elem. Anal. (calculated): C 61.95, H 8.04 %; Elem. Anal. (found): C 61.89, H 7.89 %.

Compound 6:
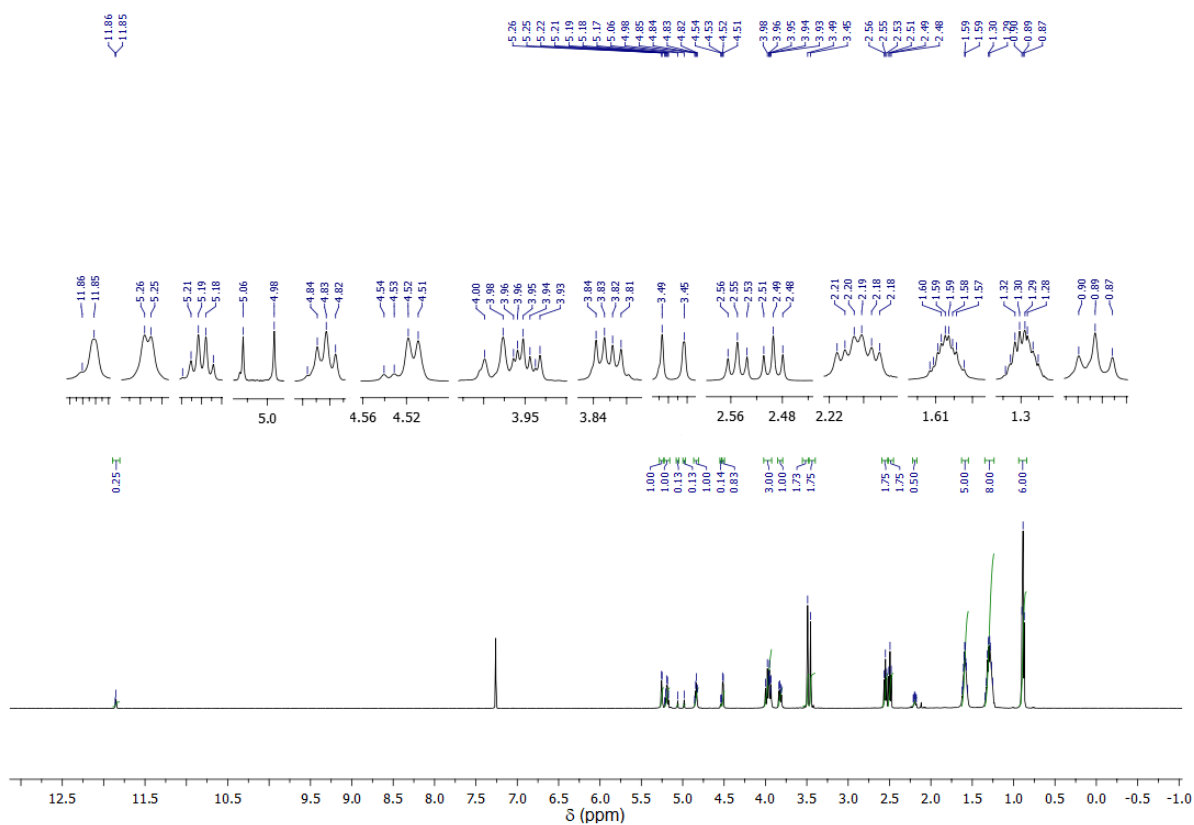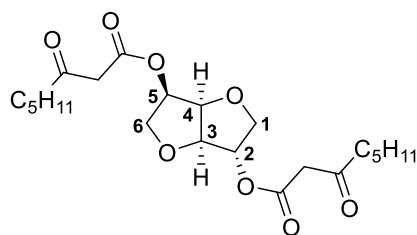
Figure S1. ^{1}H NMR spectrum (500 MHz) of **6** in CDCl$_3$.

Figure S2. ^{13}C NMR spectrum (125 MHz) of **6** in CDCl$_3$.

Figure S3. COSY spectrum of **6** in CDCl$_3$.

6
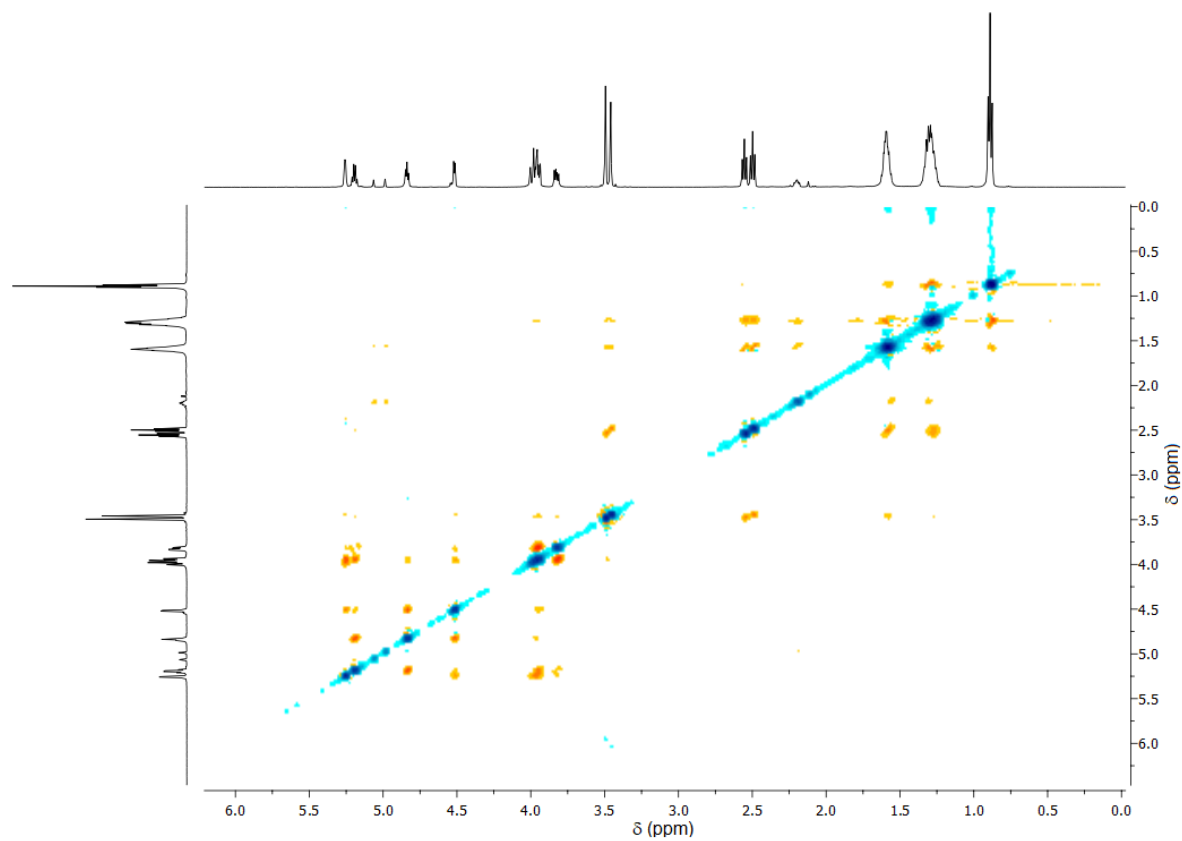
Figure S4. NOESY spectrum of **6** in CDCl₃.
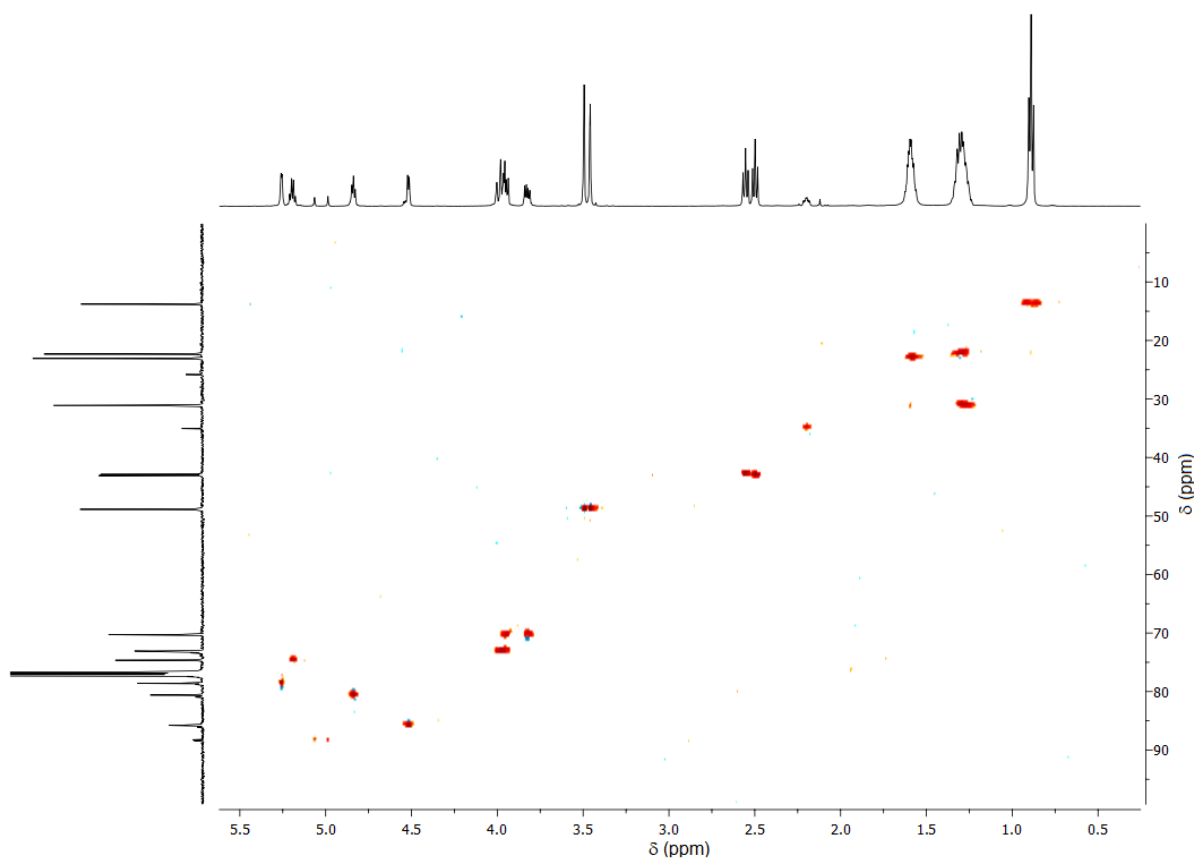
Figure S5. HSQC spectrum of **6** in CDCl₃.
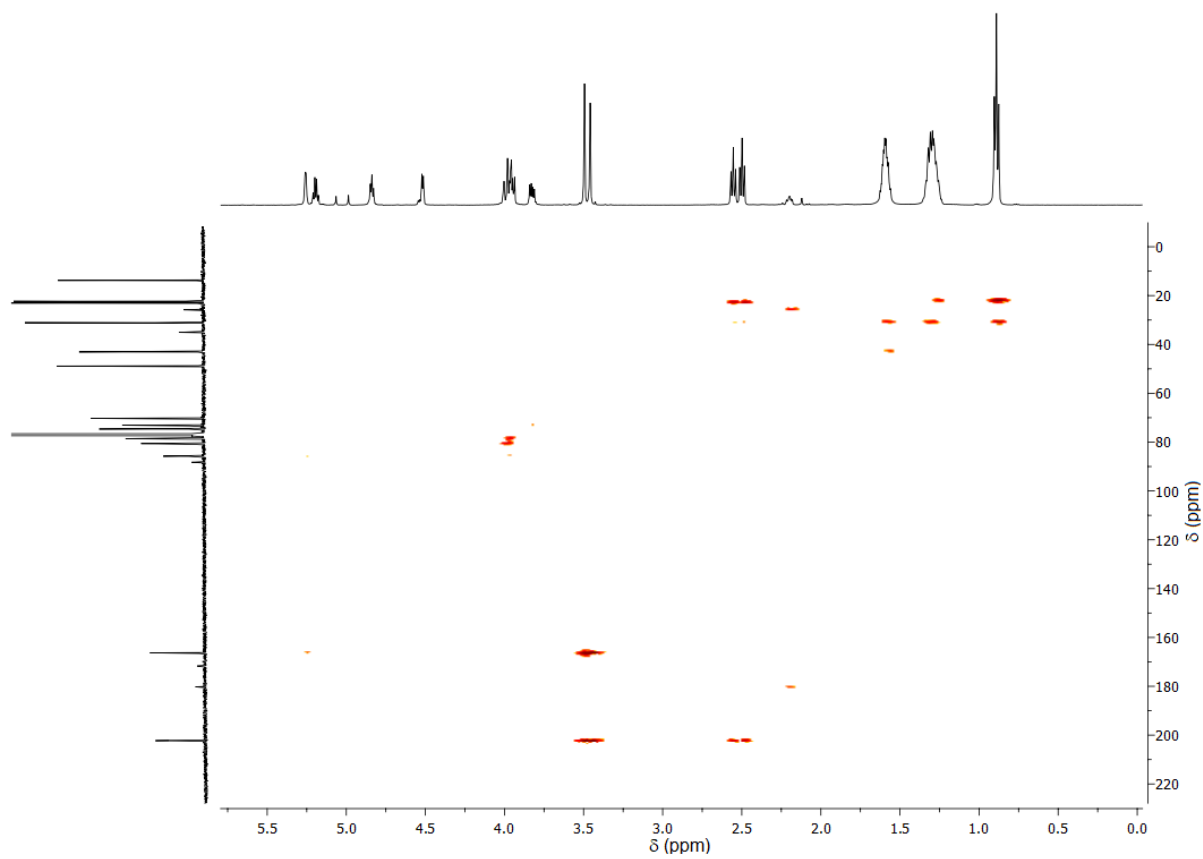
Figure S6. HMBC spectrum of **6** in CDCl₃.

Compound 8:
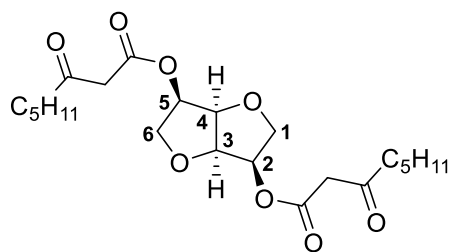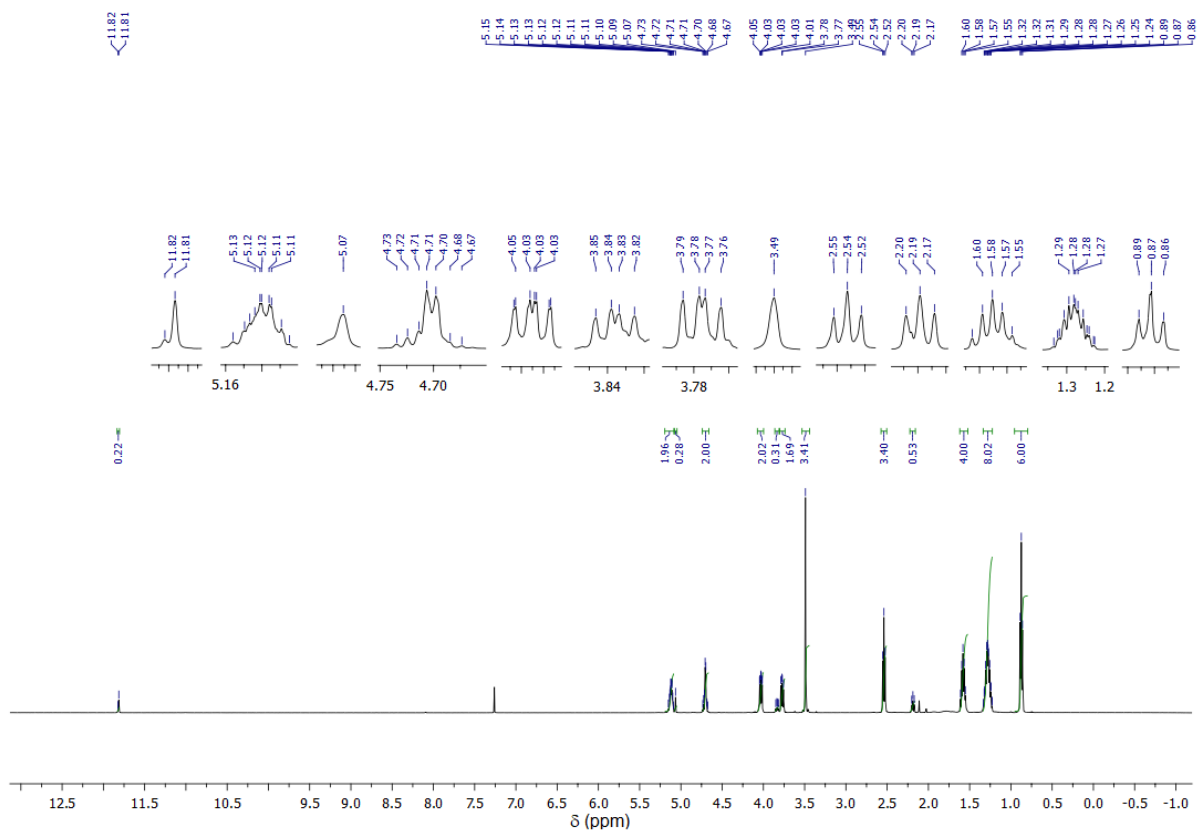
Figure S7. ¹H NMR spectrum (500 MHz) of **8** in CDCl₃.
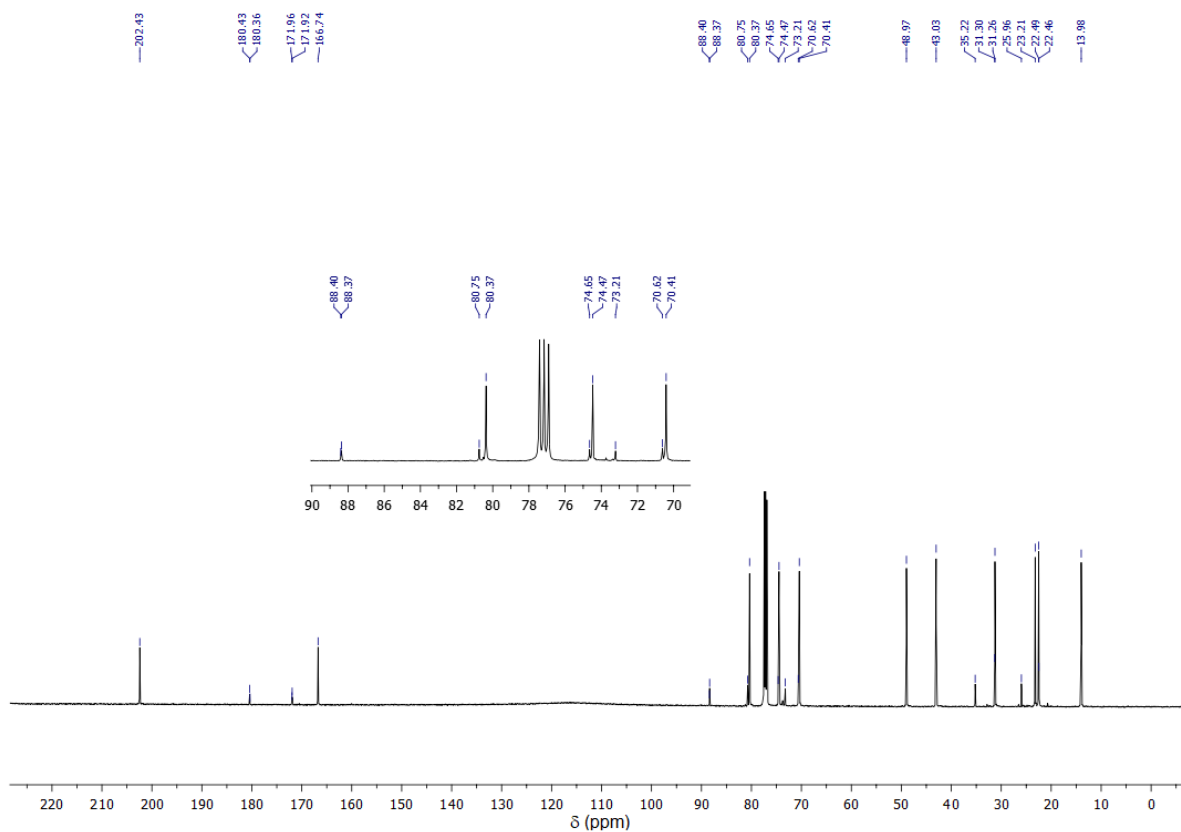
Figure S8. ¹³C NMR spectrum (125 MHz) of **8** in CDCl₃.
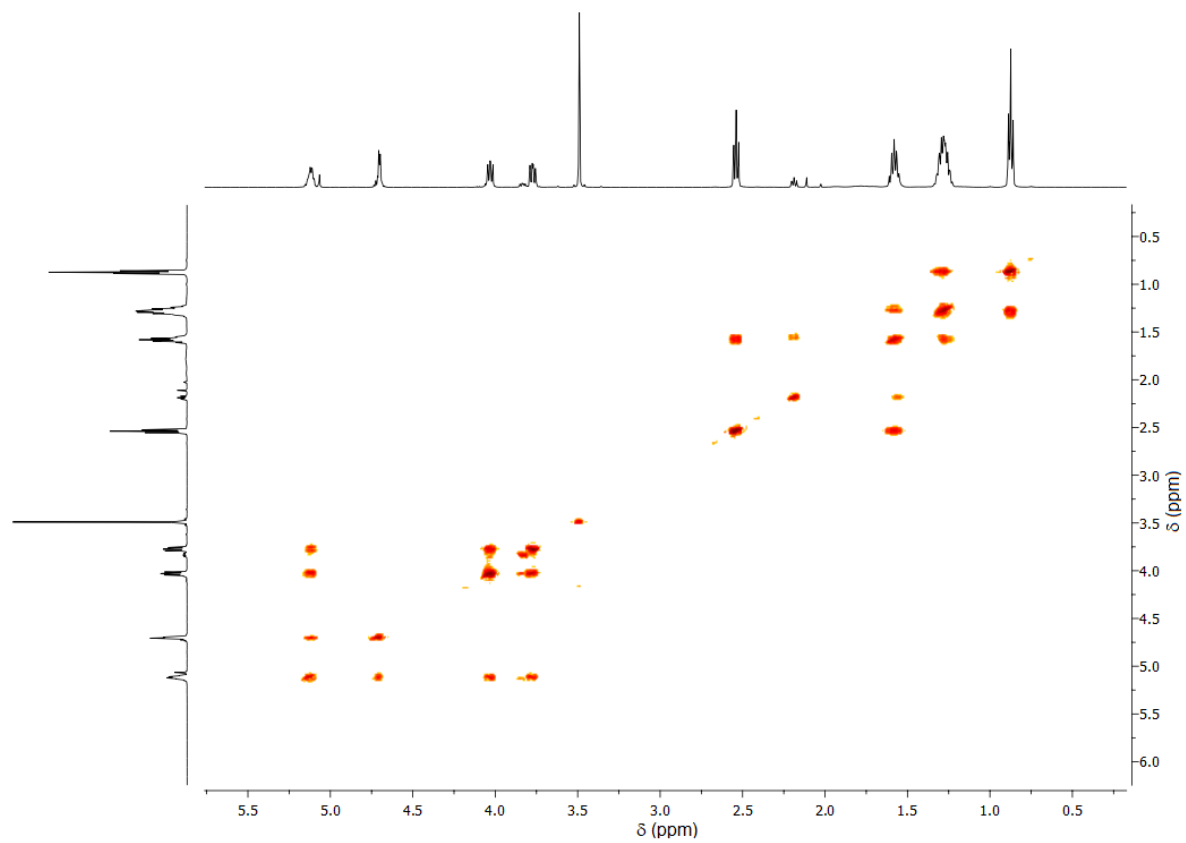
Figure S9. COSY spectrum of **8** in CDCl₃.
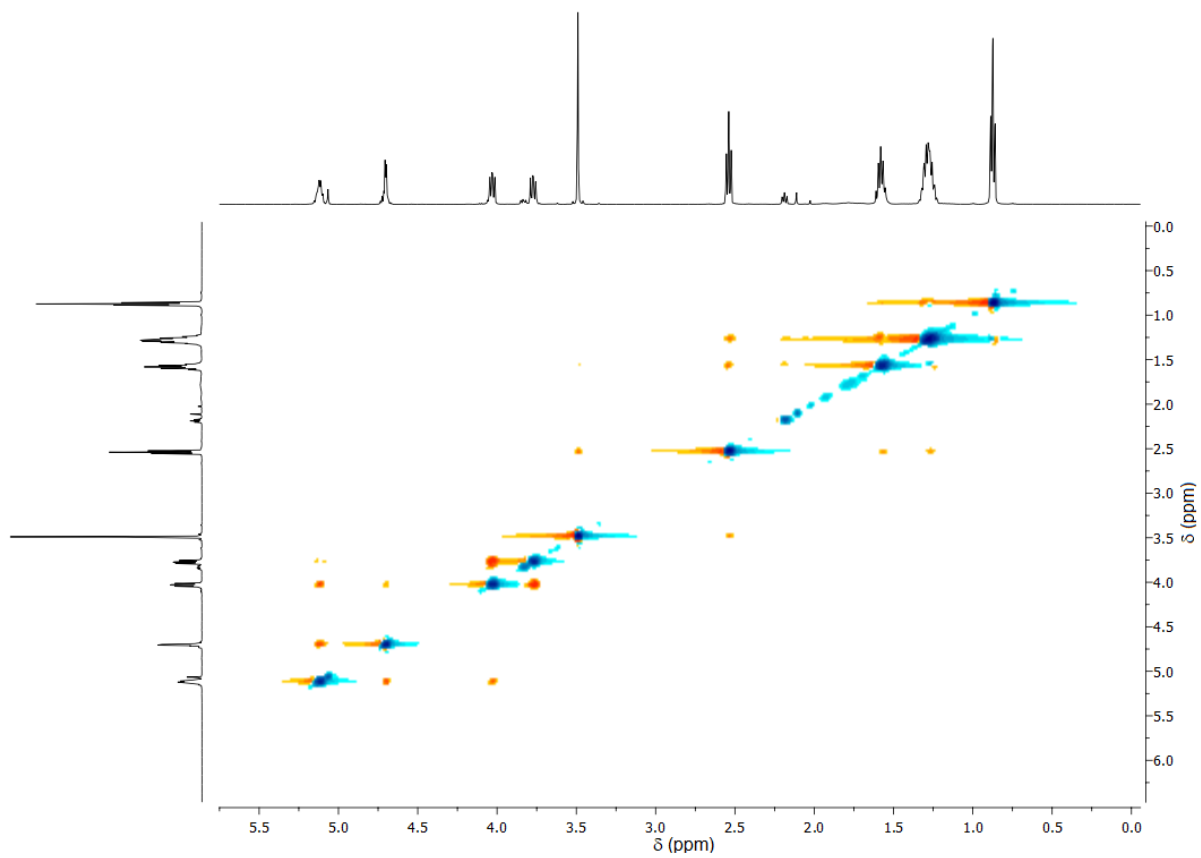
Figure S10. NOESY spectrum of **8** in CDCl₃.
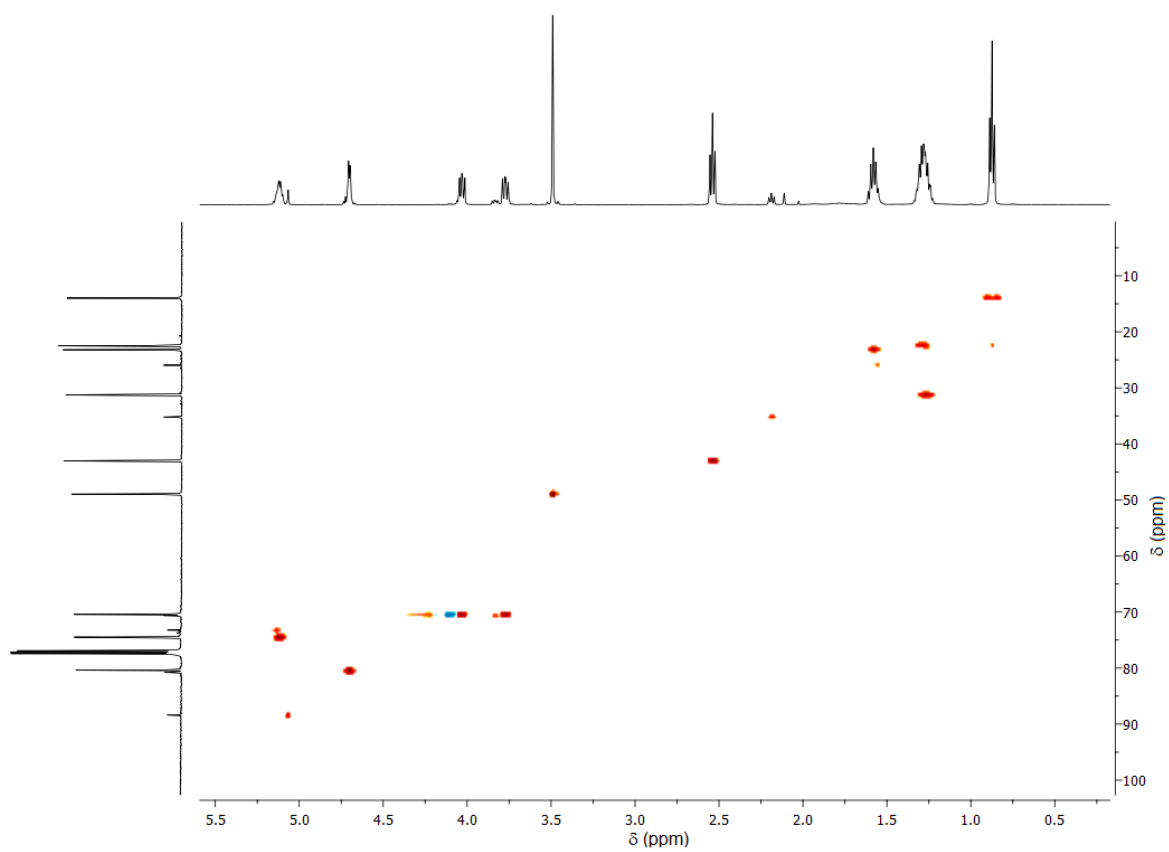
Figure S11. HSQC spectrum of **8** in CDCl₃.
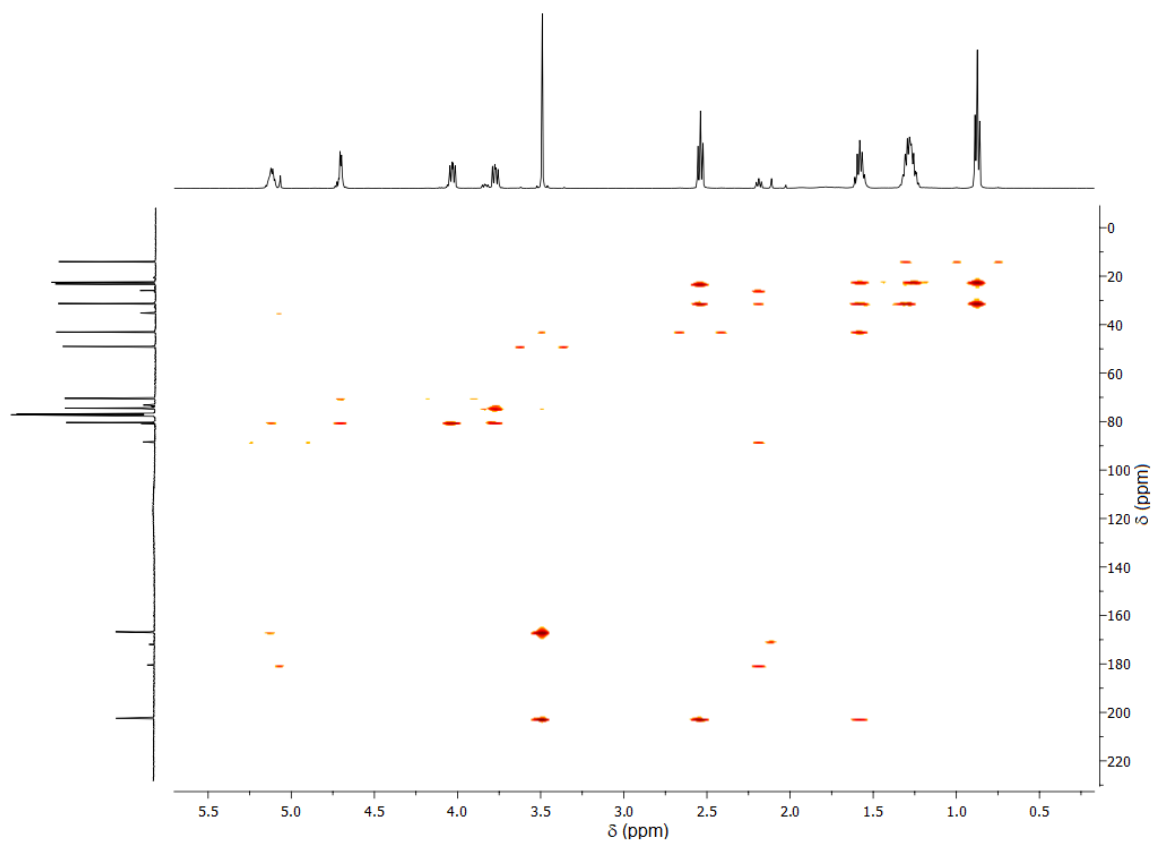
Figure 12. HMBC spectrum of **8** in CDCl₃.

Compound 10IS:

Figure S13. ^{1}H NMR spectrum (400 MHz) of **10IS** in CDCl$_3$/CS$_2$.
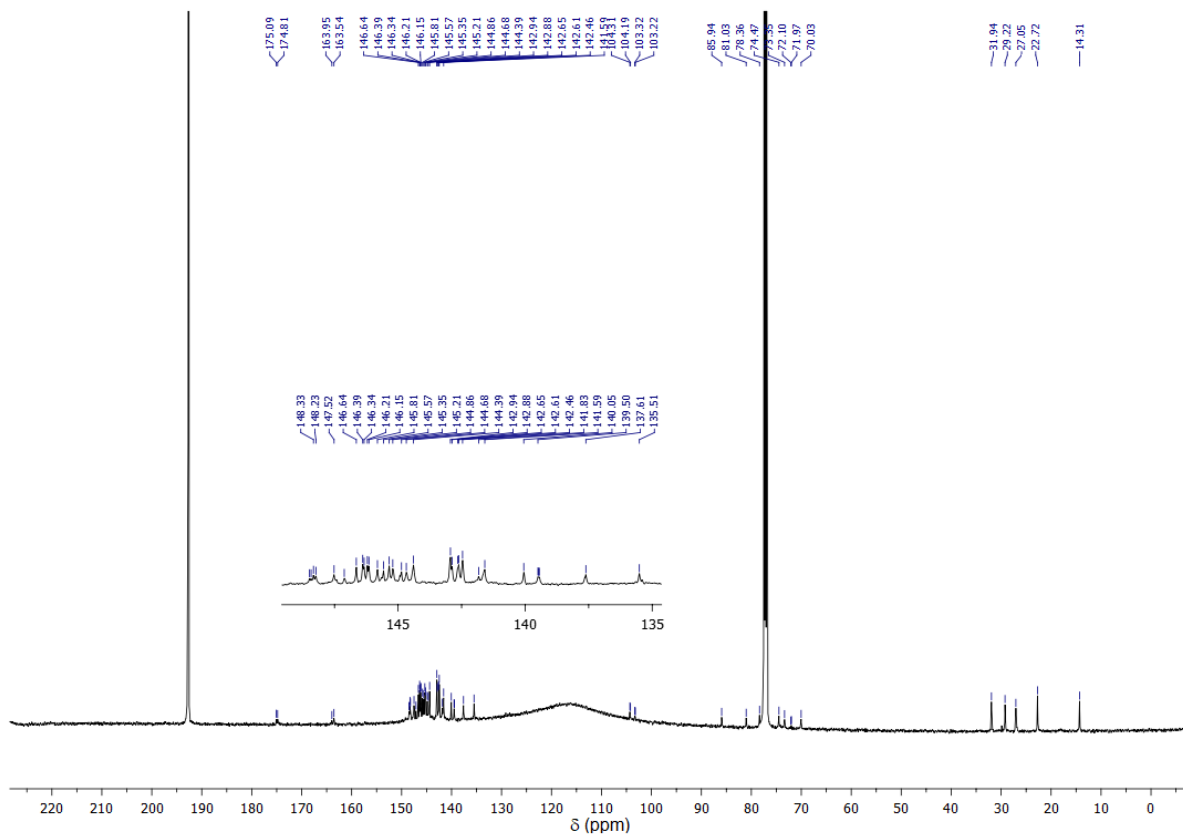
Figure S14. ^{13}C NMR spectrum (100 MHz) of **10$_{IS}$** in CDCl$_3$/CS$_2$.
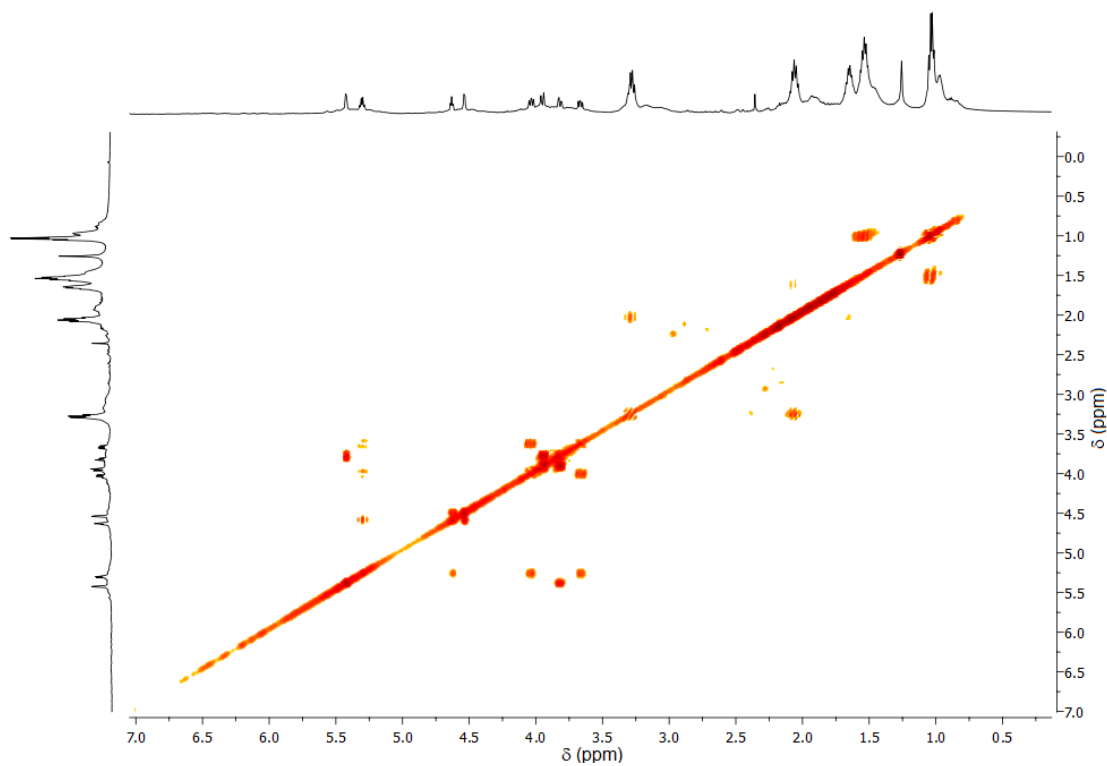
Figure S15. COSY spectrum of **10$_{IS}$** in CDCl$_3$/CS$_2$.

13
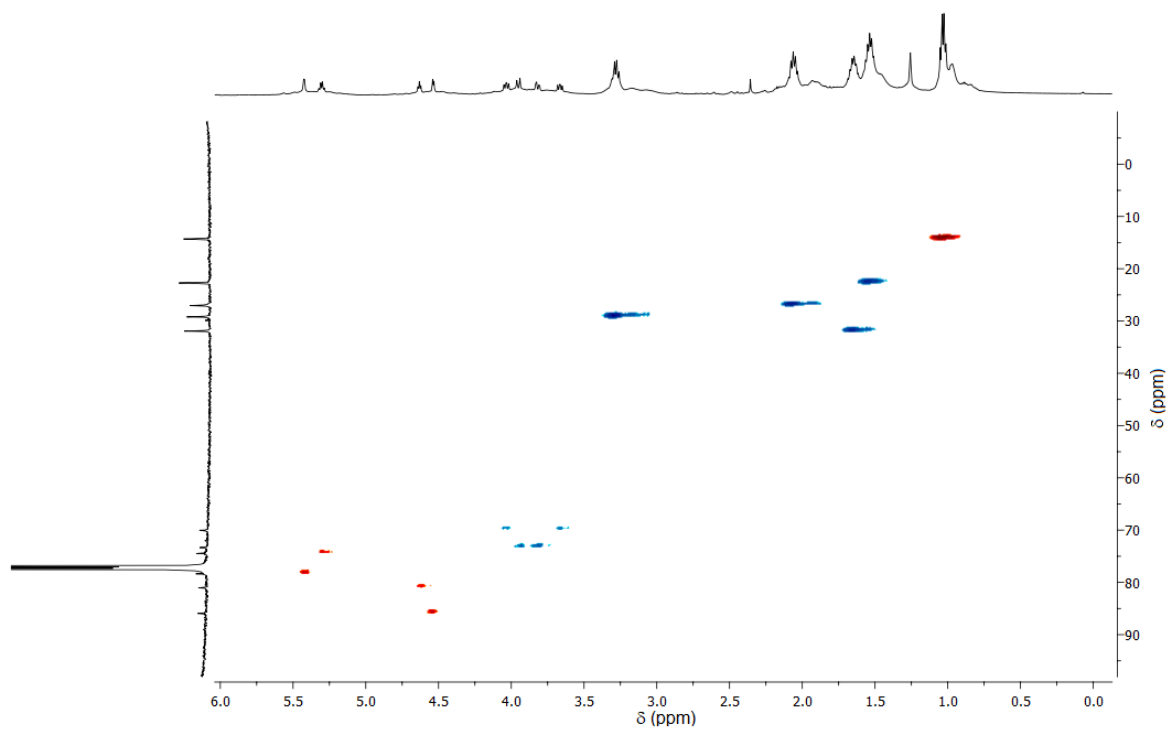
Figure S16. HSQC spectrum of **10$_{IS}$** in CDCl$_3$/CS$_2$.
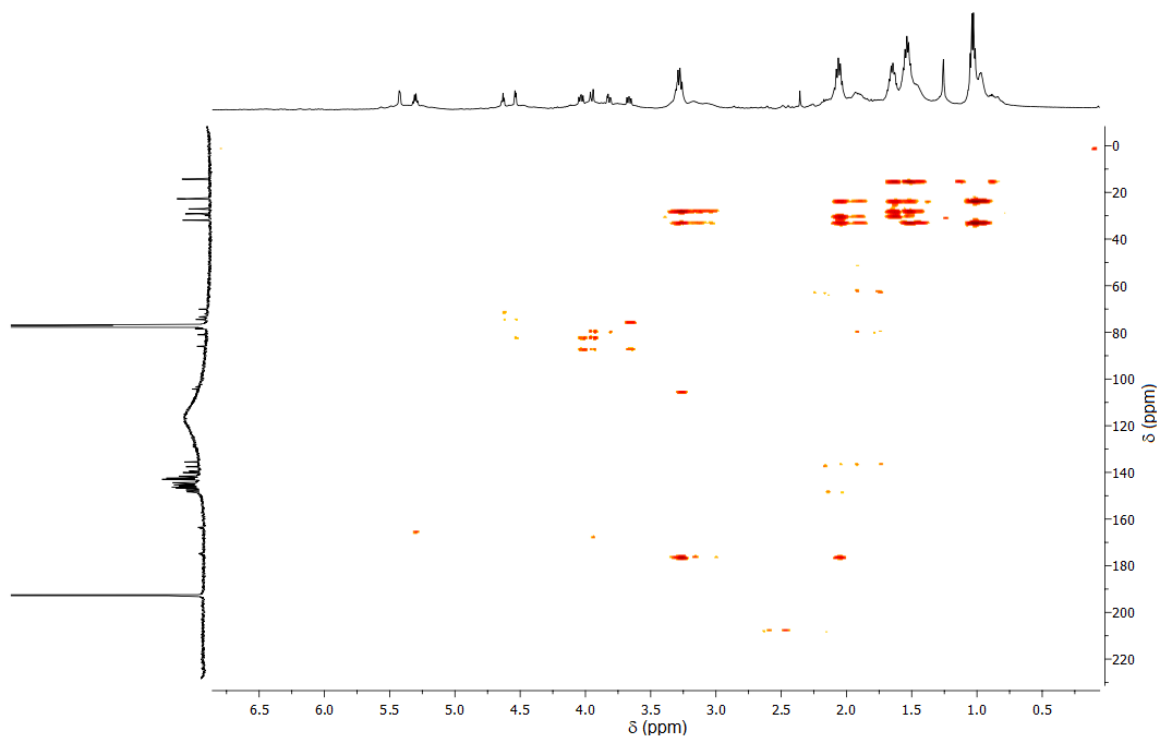
Figure S17. HMBC spectrum of **10$_{IS}$** in CDCl$_3$/CS$_2$.
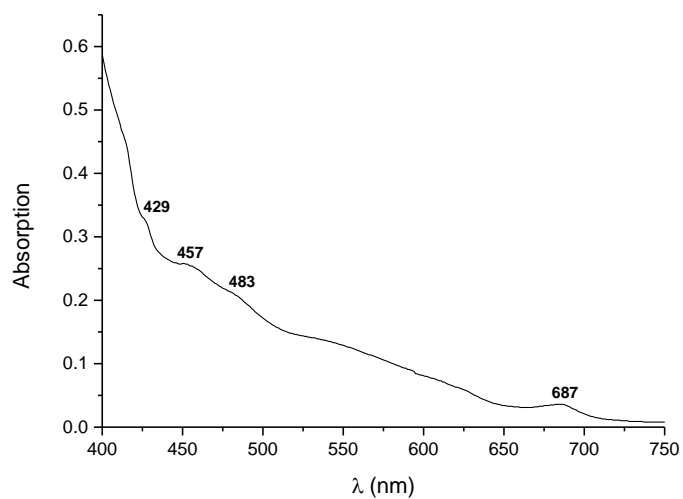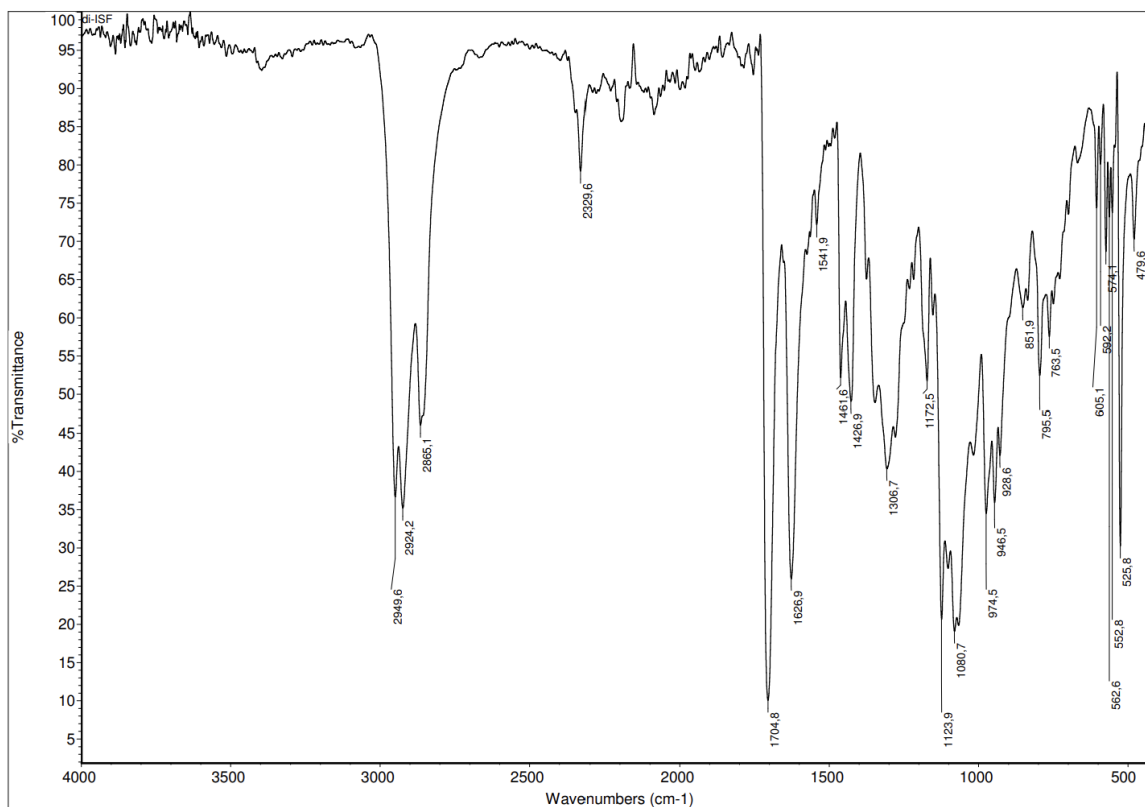
Figure S18. a) UV-vis absorption spectrum of **10₁ₛ** compound in CHCl₃. b) FTIR-ATR of **10₁ₛ**.

Compound 11_{IM}:
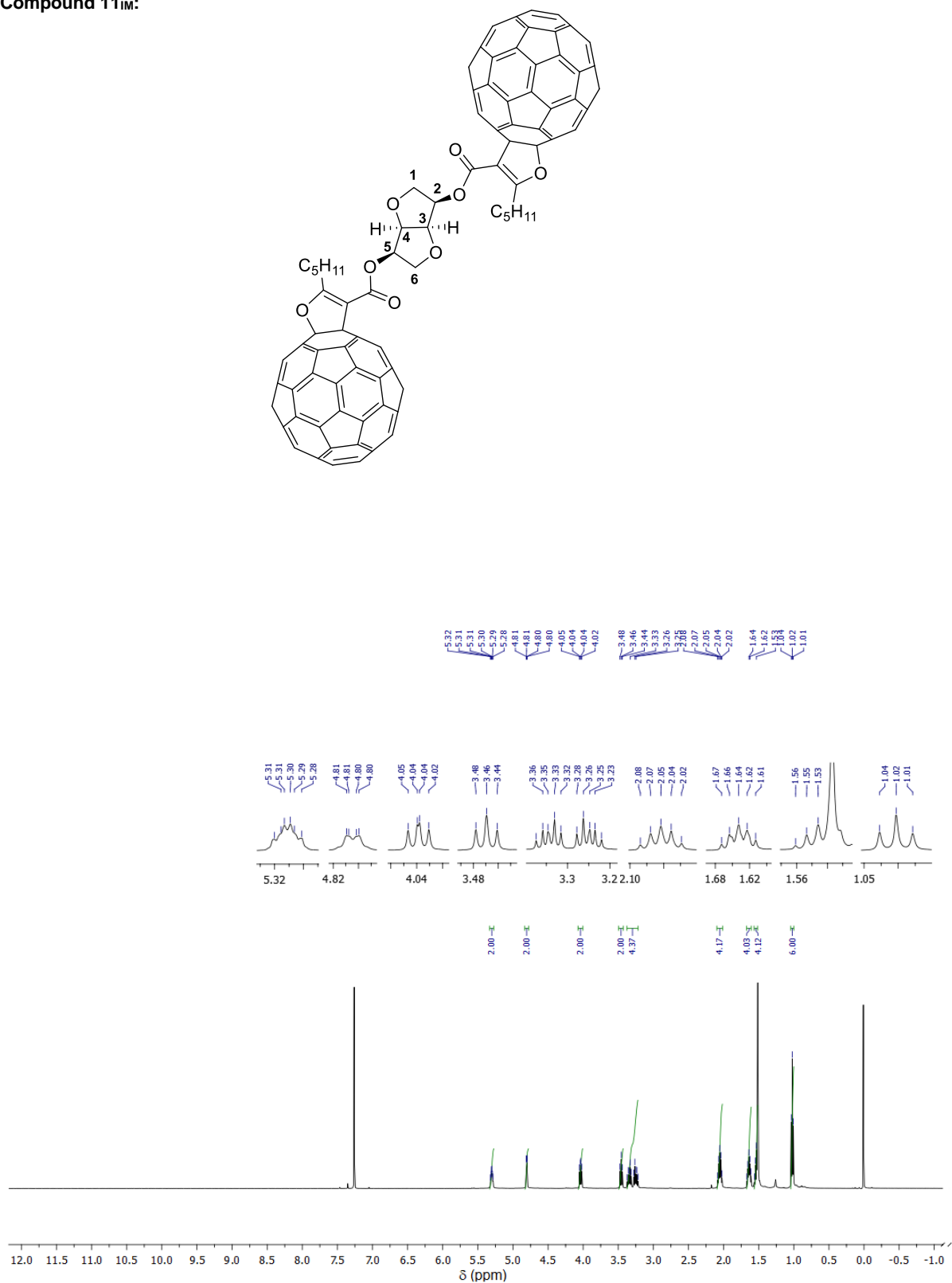
Figure S19. ^{1}H NMR spectrum (500 MHz) of **11**_{IM} in CDCl$_3$/CS$_2$.
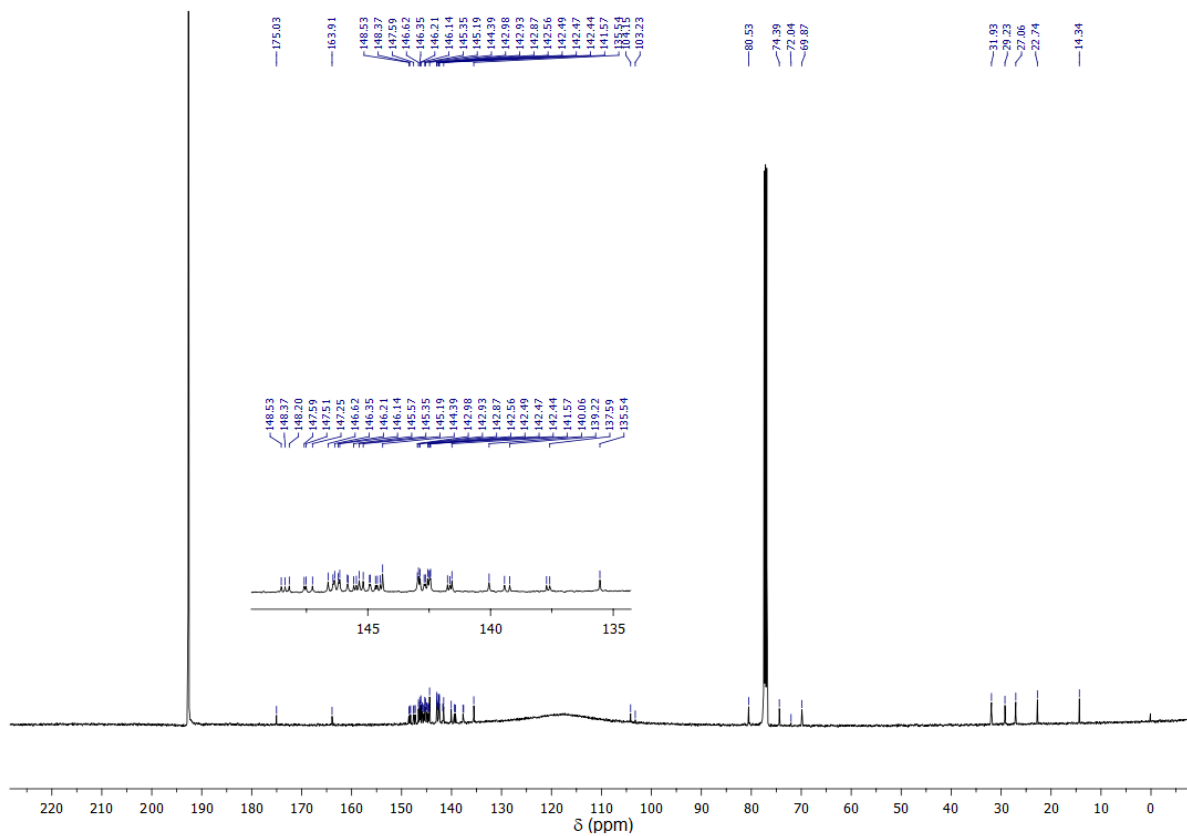
Figure S20. ^{13}C NMR spectrum (125 MHz) of **11$_{IM}$** in CDCl$_3$/CS$_2$.
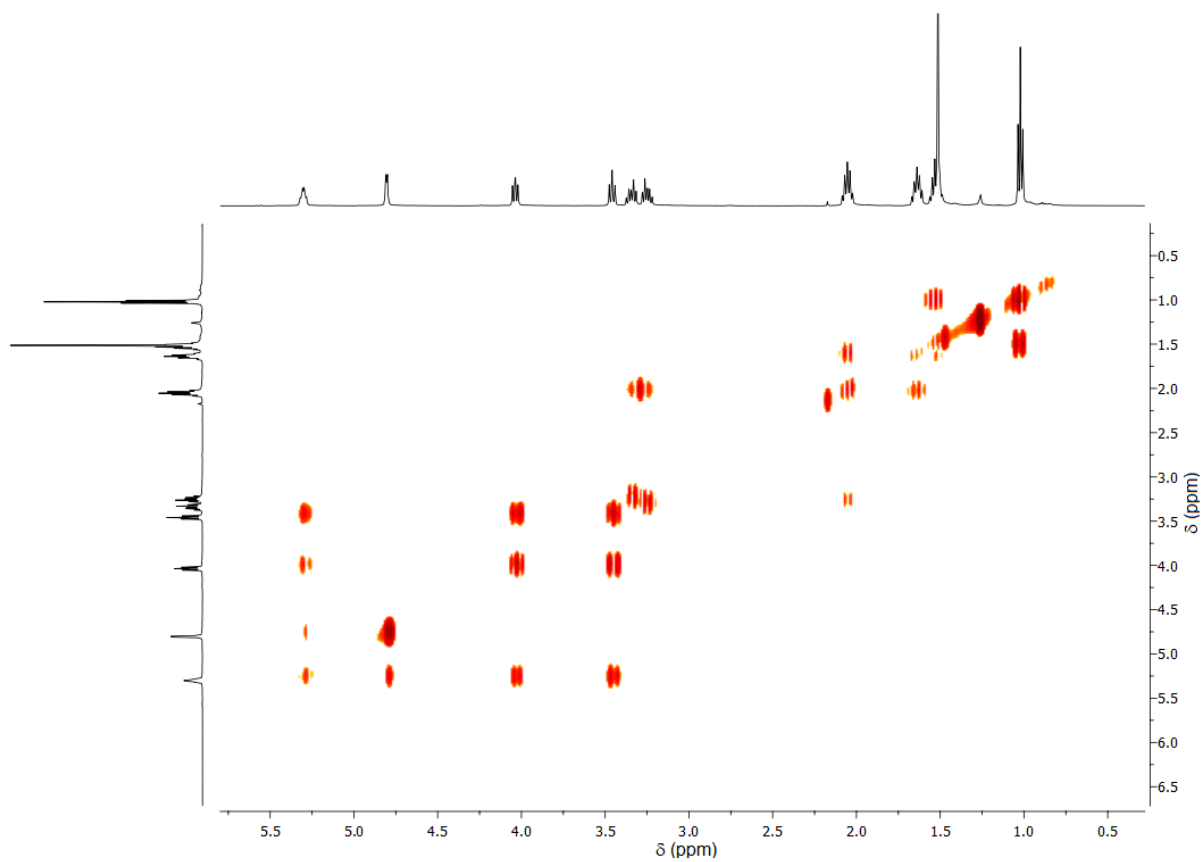
Figure S21. COSY spectrum of **11$_{IM}$** in CDCl$_3$/CS$_2$.
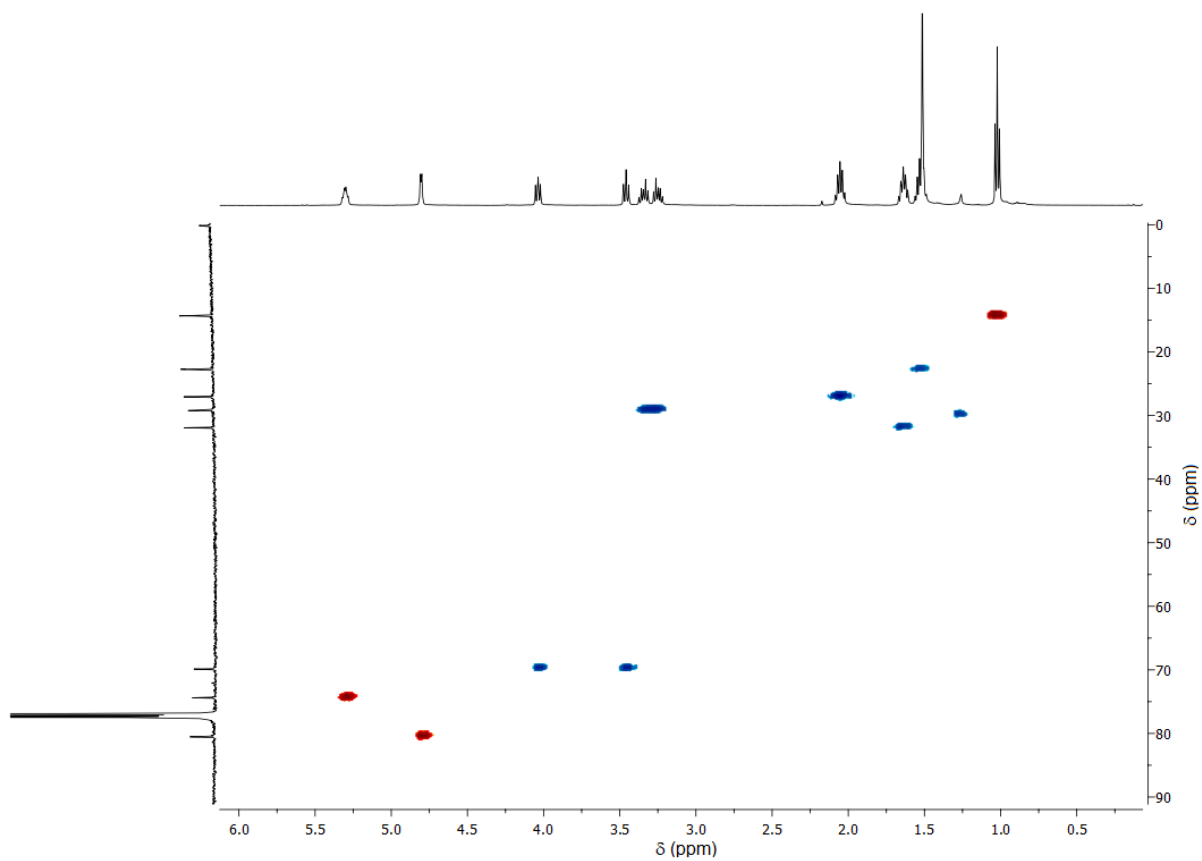
Figure S22. HSQC spectrum of **11ᴵᴹ** in CDCl₃/CS₂.
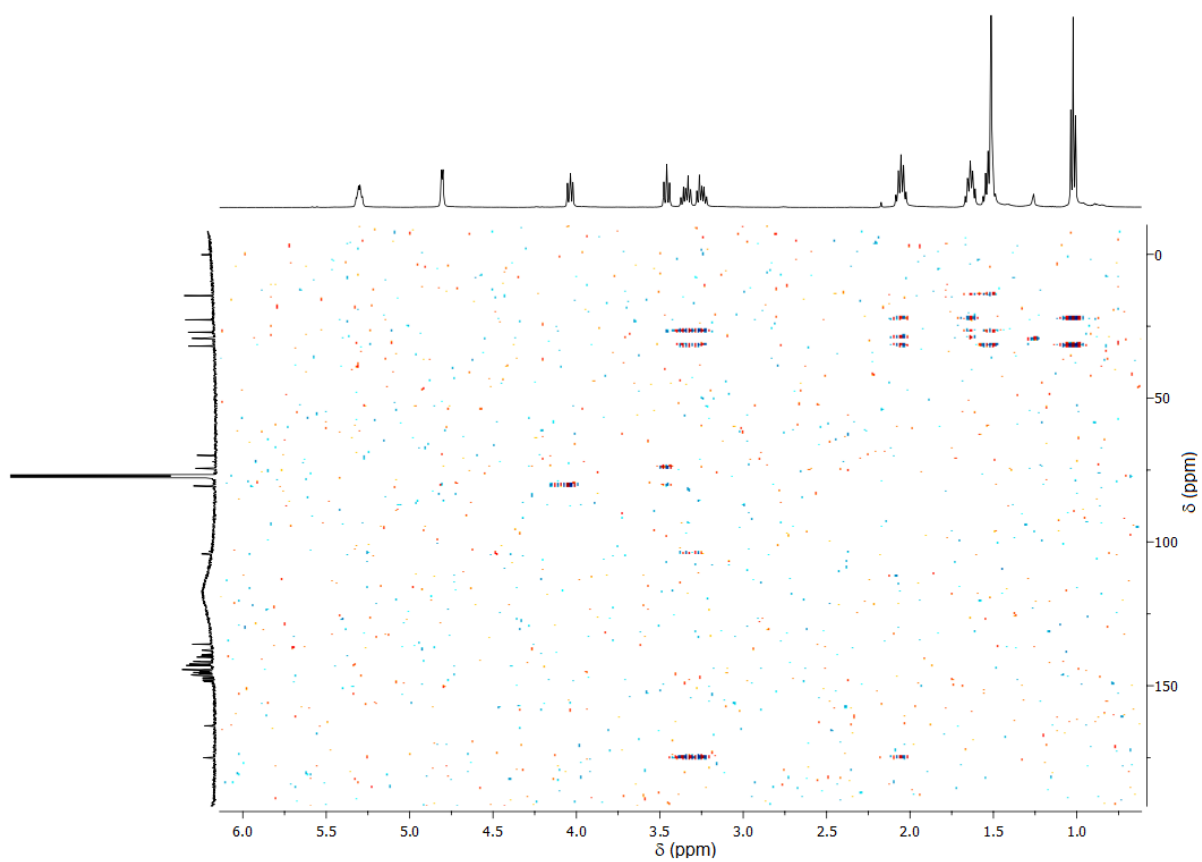
Figure S23. HMBC spectrum of **11ᴵᴹ** in CDCl₃/CS₂.

a)
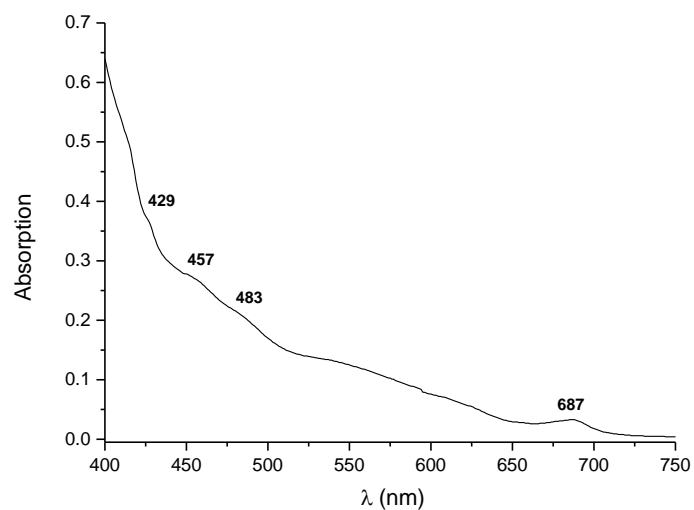
λ (nm)	ε (dm^3 mol^{-1} cm^{-1})
429	8756
457	6642
483	5224
687	821

b)
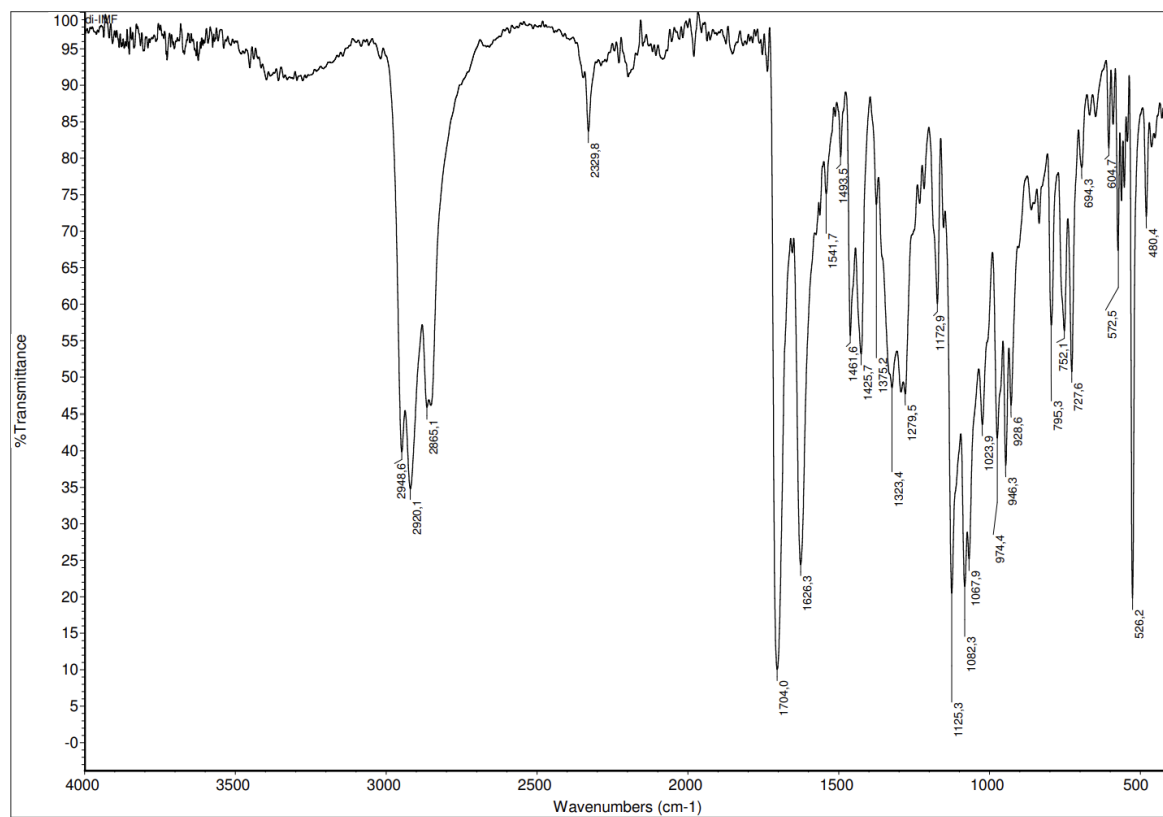
Figure S24. a) UV-vis absorption spectrum of compound **11$_{IM}$** in CHCl$_3$. b) FTIR-ATR of **11$_{IM}$**.

Compound 12ₗₛ:
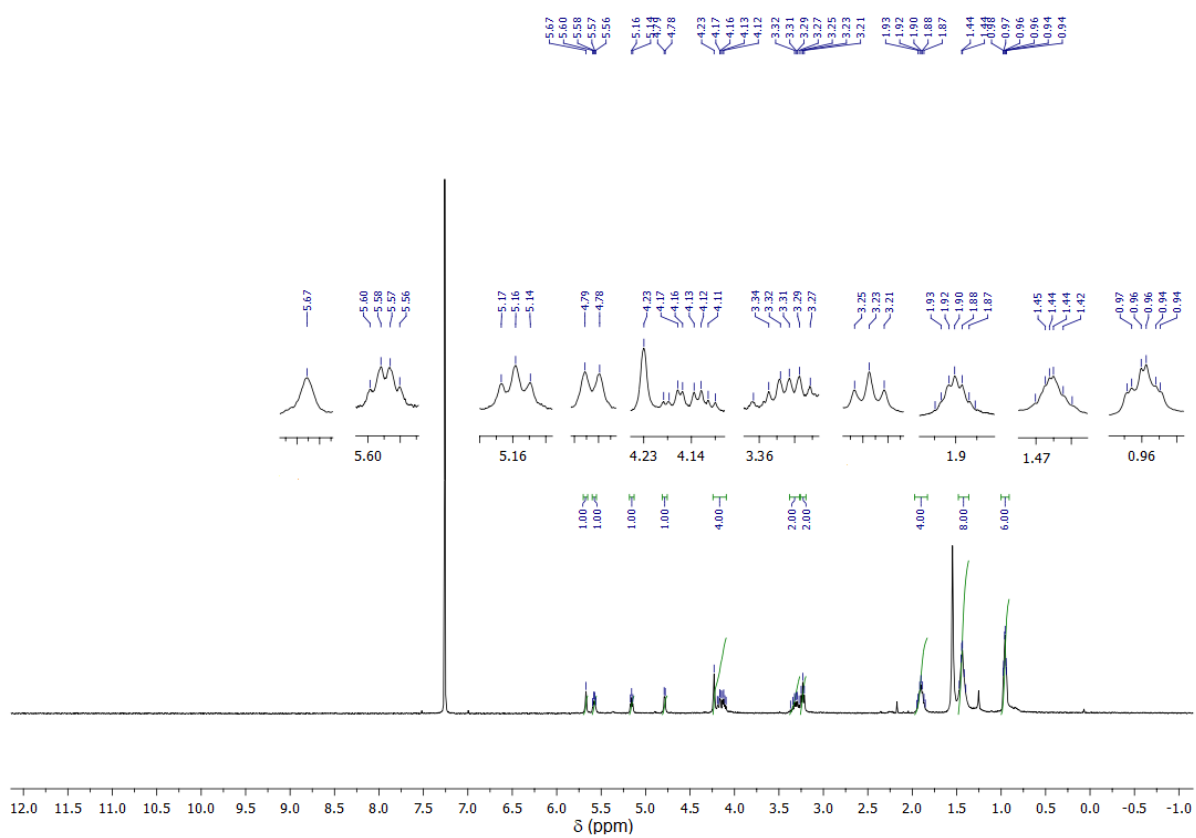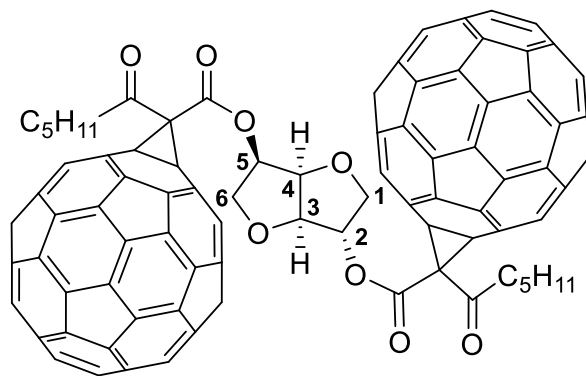
Figure S25. ¹H NMR spectrum (400 MHz) of **12ₗₛ** in CDCl₃.
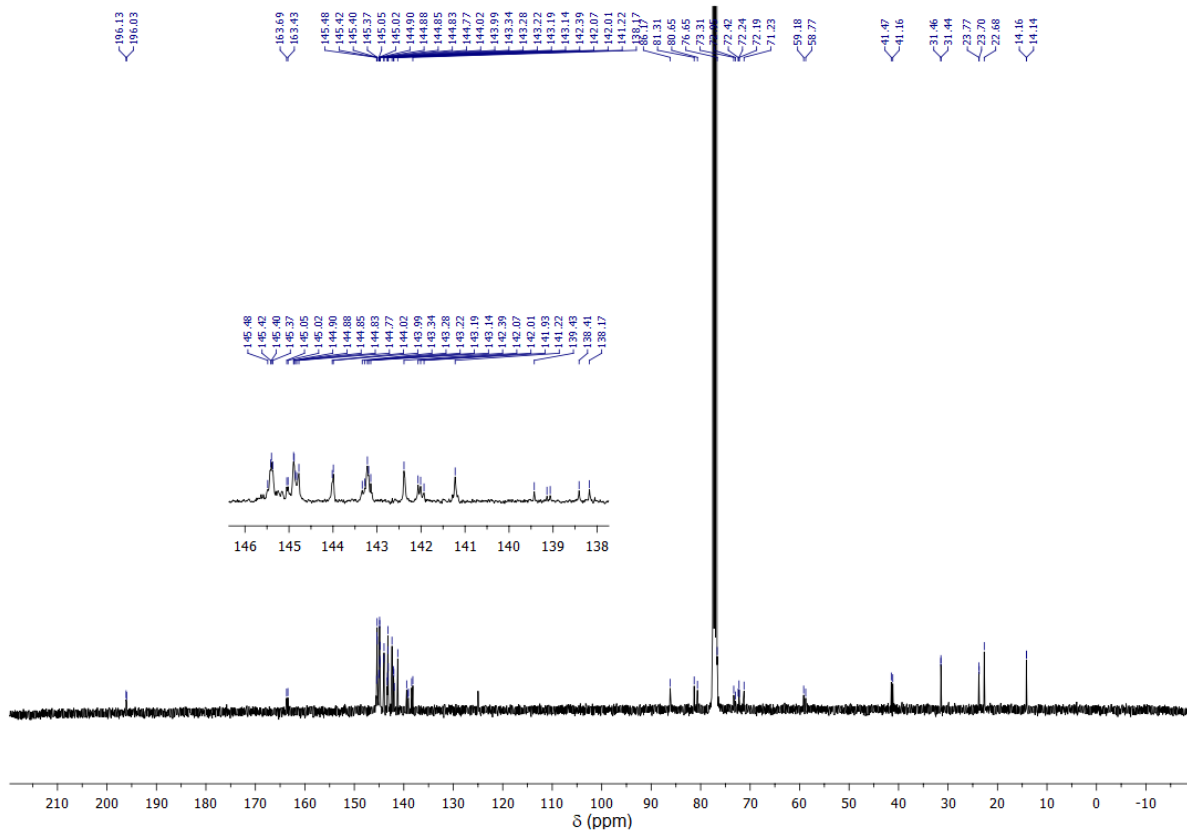
Figure S26. ^{13}C NMR spectrum (100 MHz) of **12$_{IS}$** in CDCl$_3$.
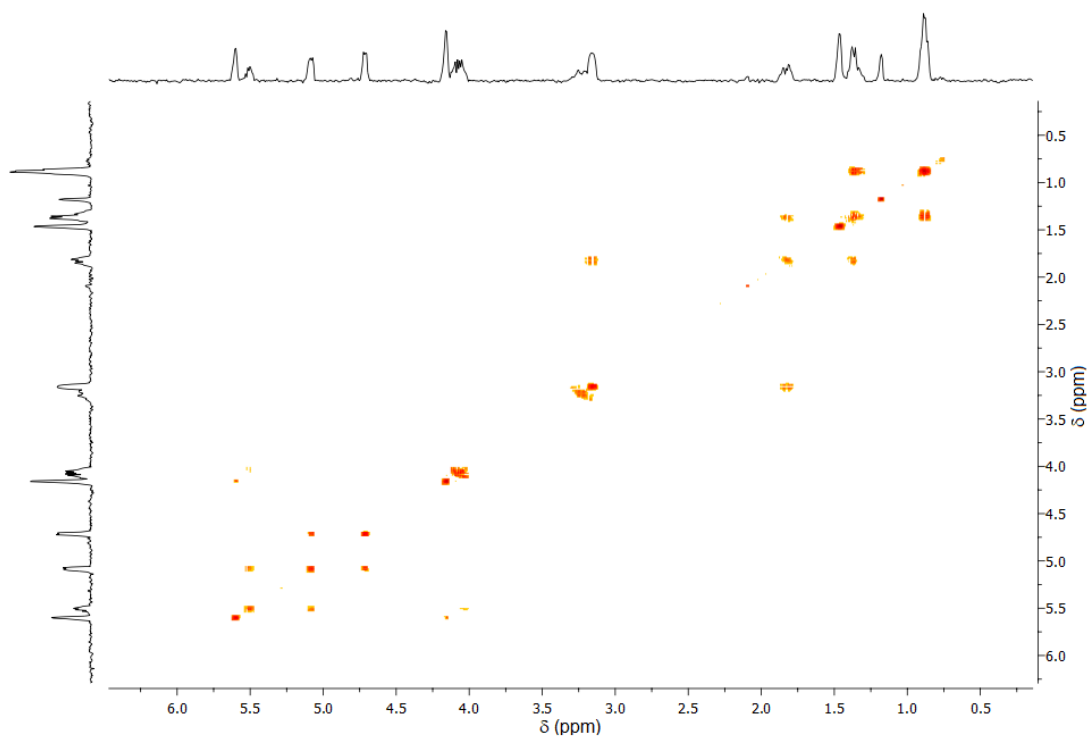
Figure S27. COSY spectrum of **12$_{IS}$** in CDCl$_3$.
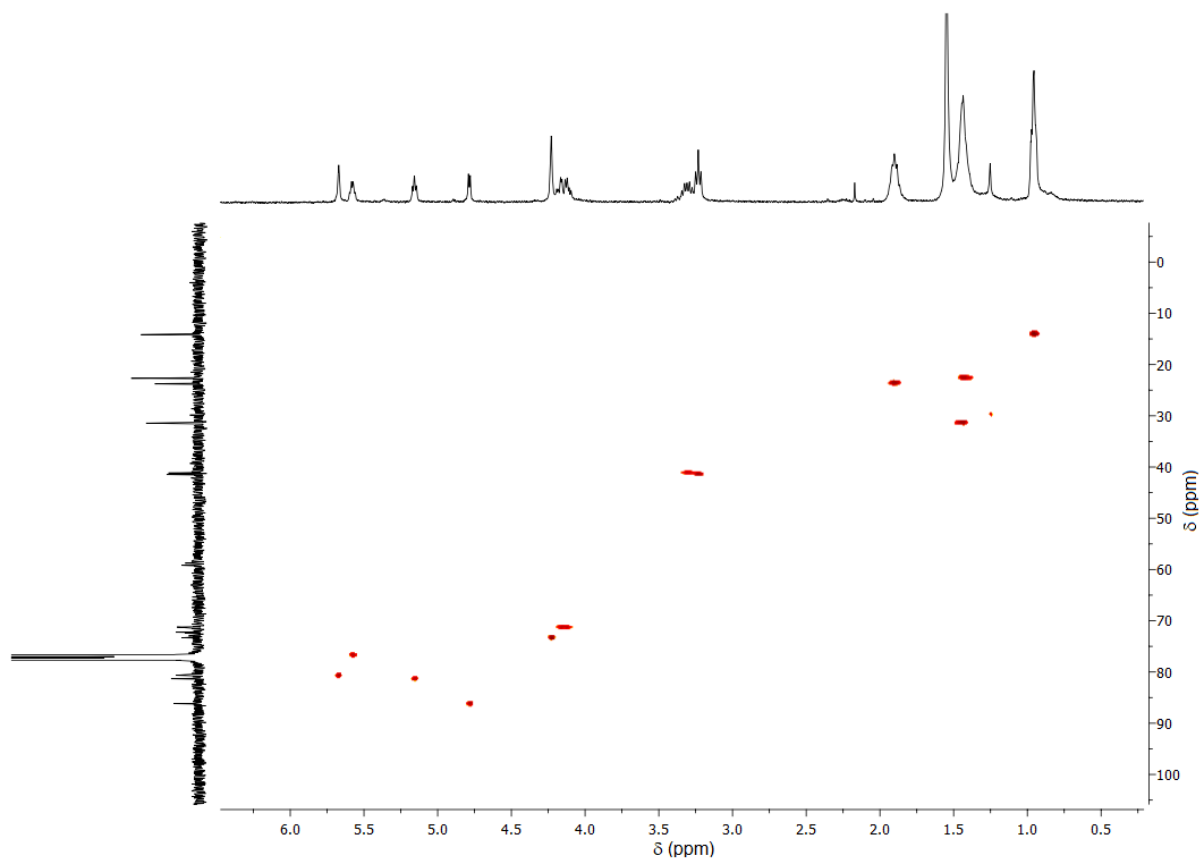
Figure S28. HSQC spectrum of **12ıs** in CDCl₃.
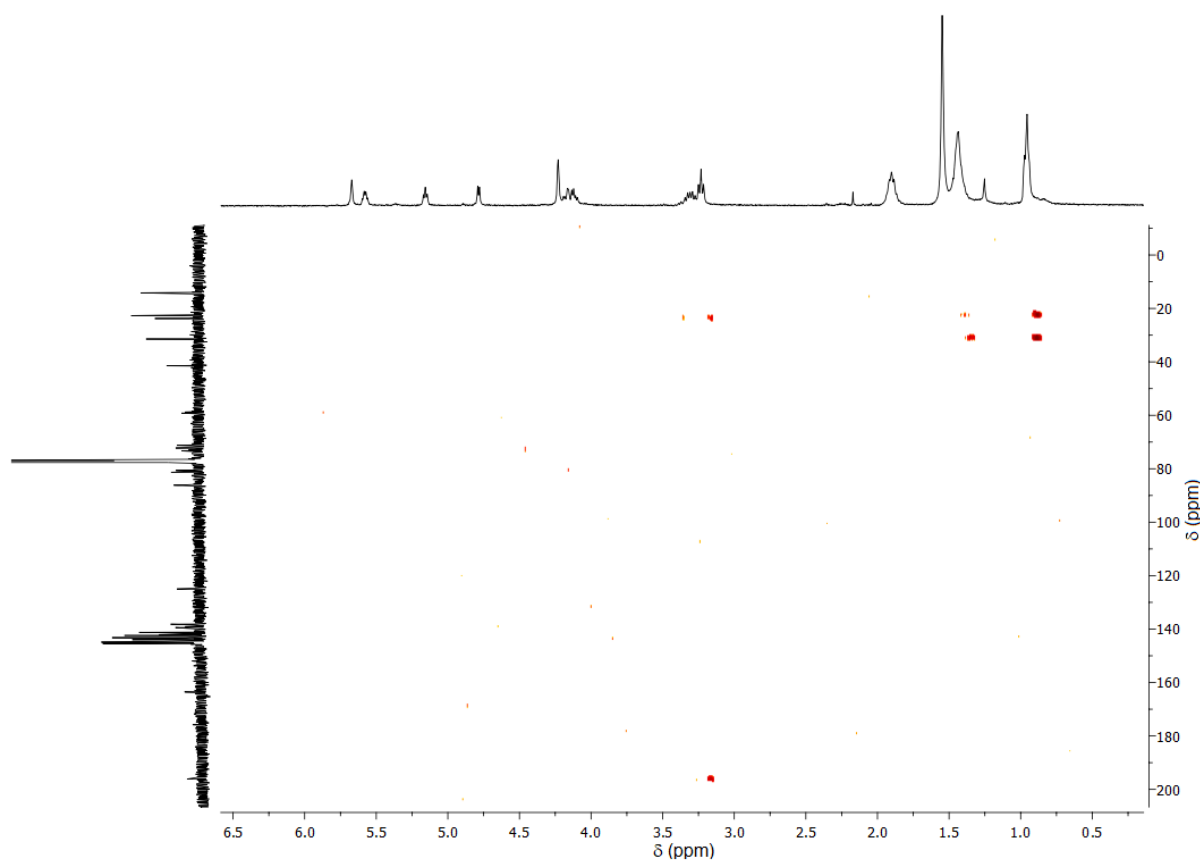
Figure S29. HMBC spectrum of **12ıs** in CDCl₃.

a)
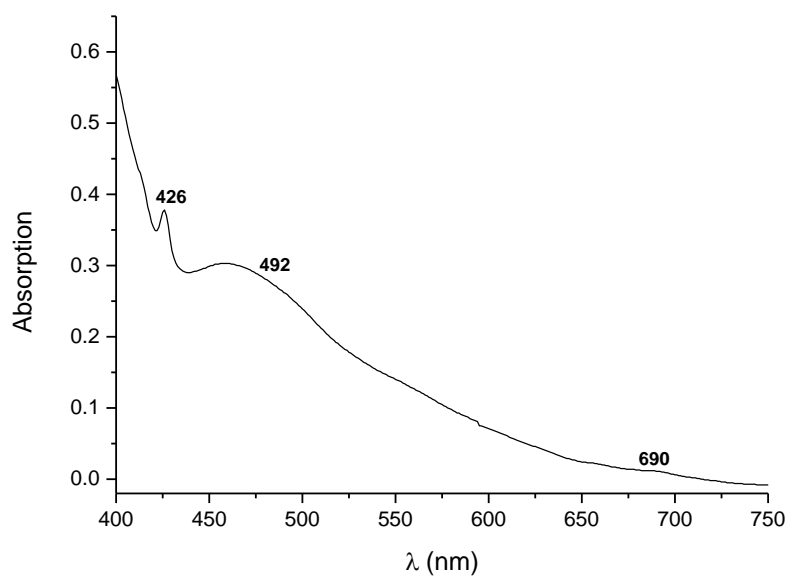
λ (nm)	ε (dm^3 mol^{-1} cm^{-1})
426	7052
492	4832
690	205

b)
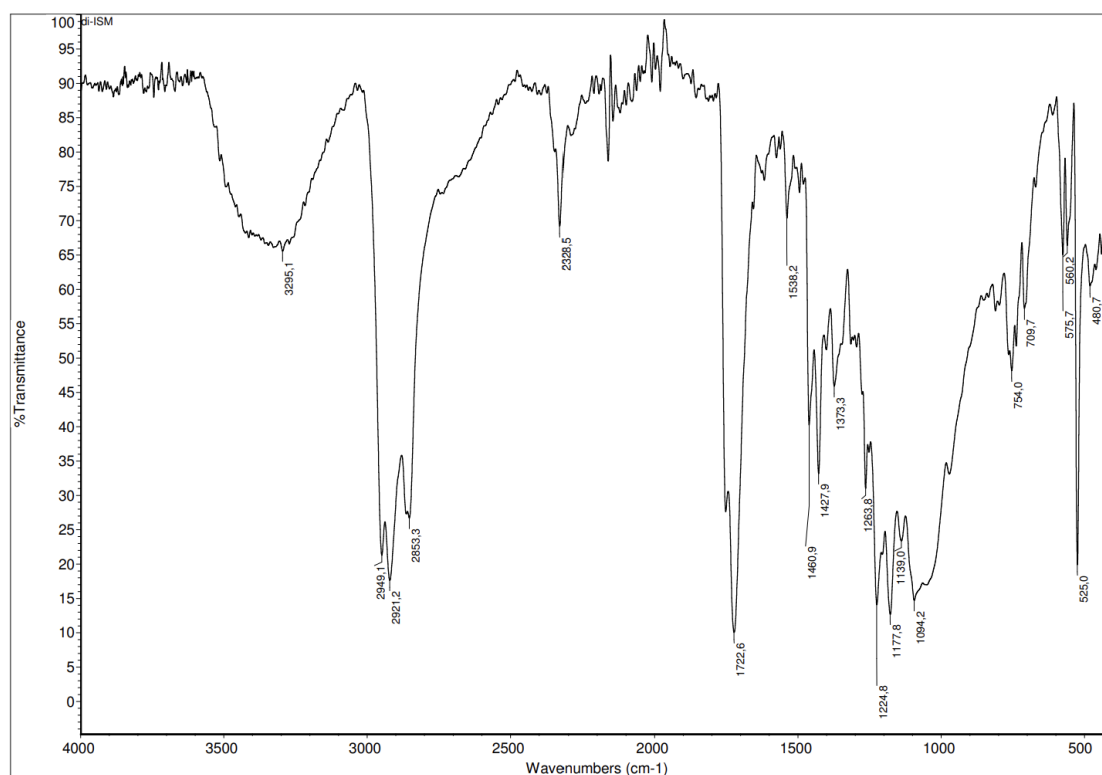
Figure S30. UV-vis absorption spectrum of **12$_{IS}$** compound in CHCl$_3$. b) FTIR-ATR of **12$_{IS}$**.

Compound 13_{IM}:
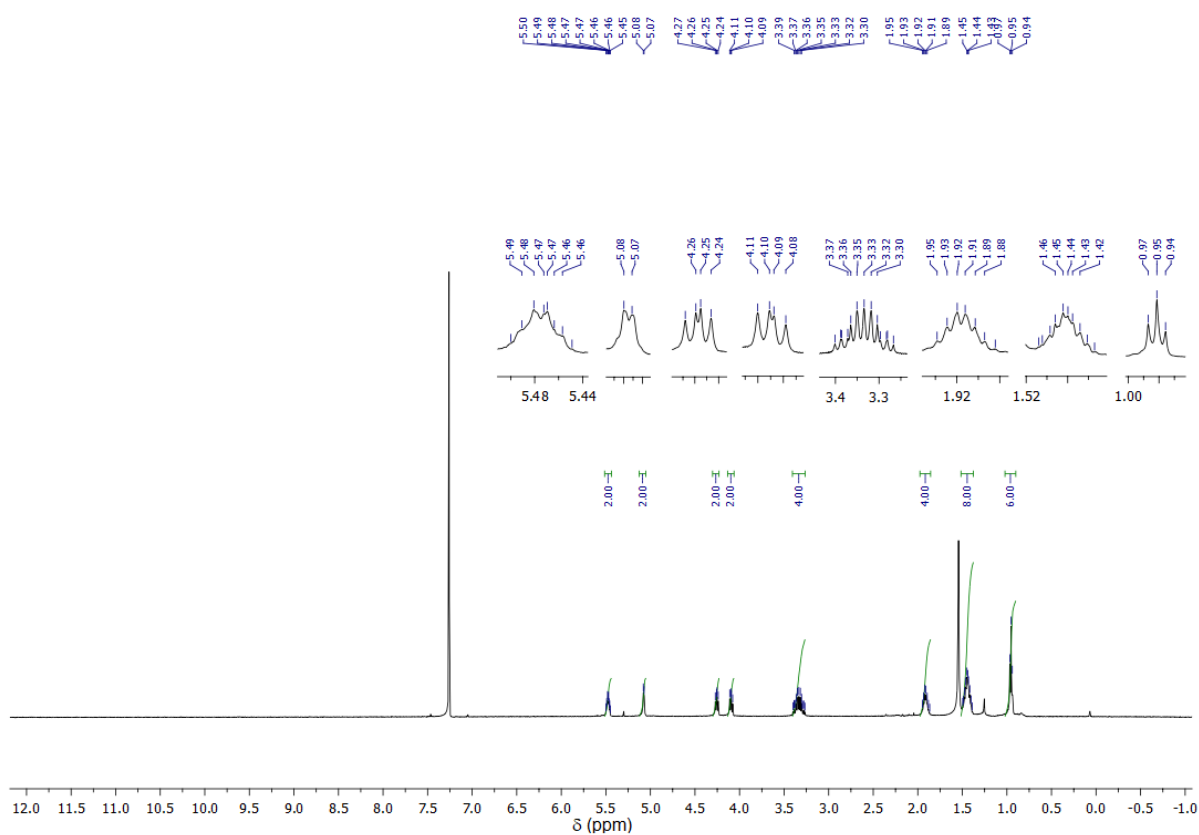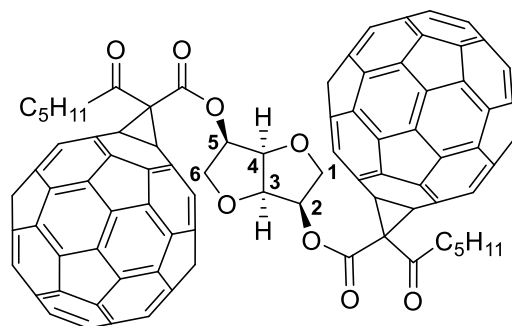
Figure S31. ^{1}H NMR spectrum (500 MHz) of **13_{IM}** in CDCl$_3$.
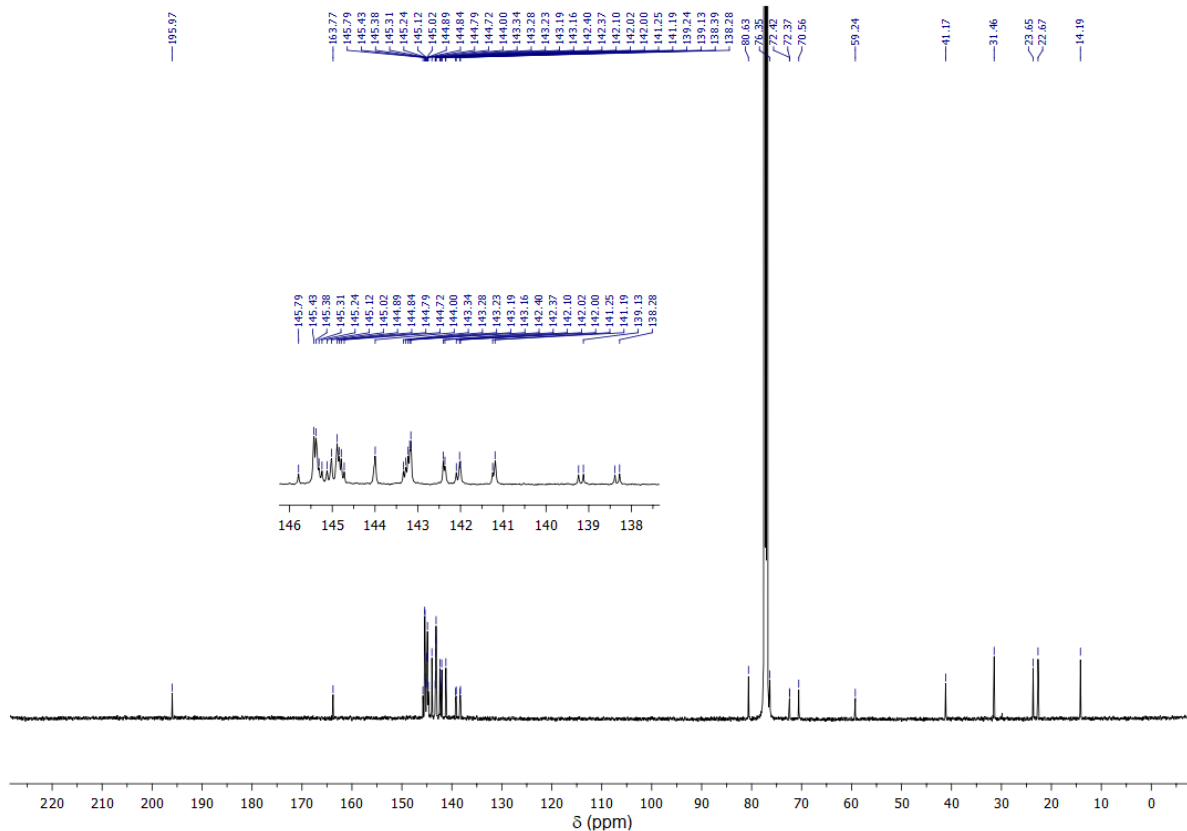
Figure S32. ^{13}C NMR spectrum (125 MHz) of **13$_{IM}$** in CDCl$_3$.
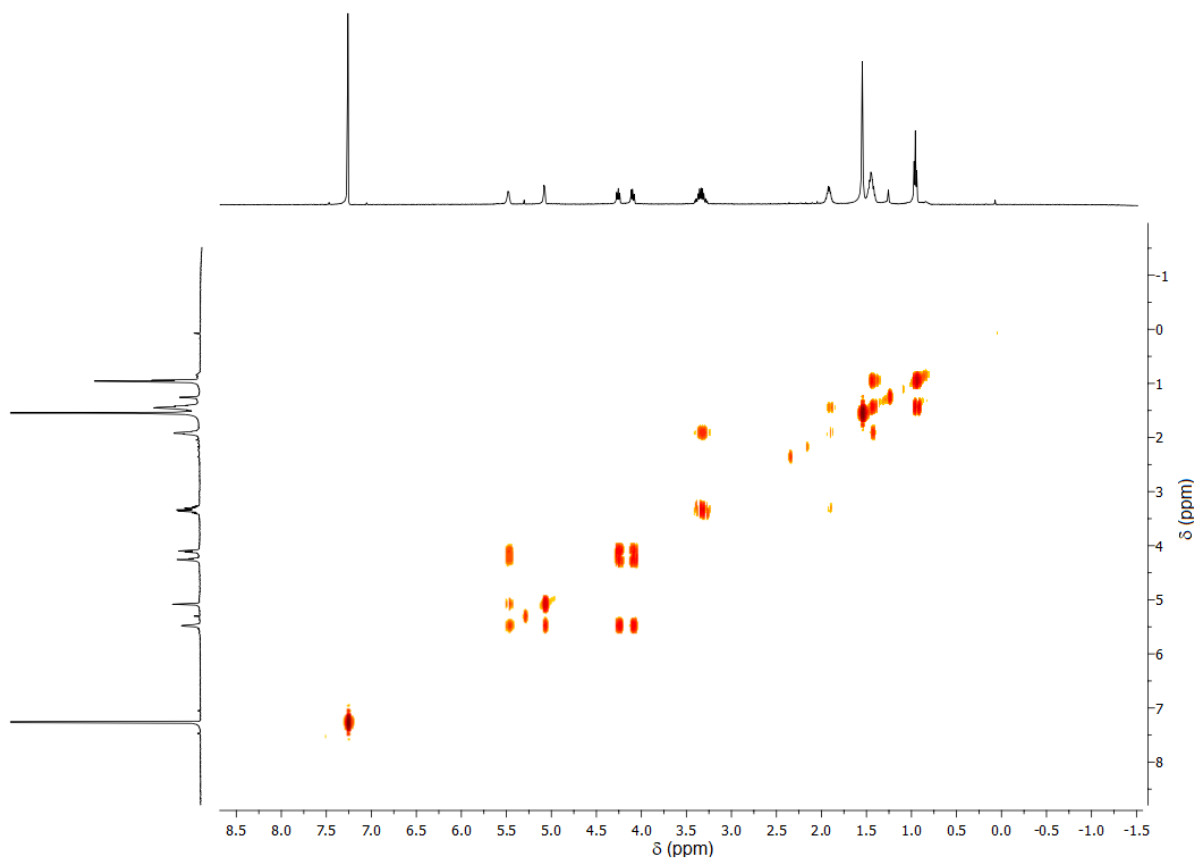
Figure S33. COSY spectrum of **13$_{IM}$** in CDCl$_3$.
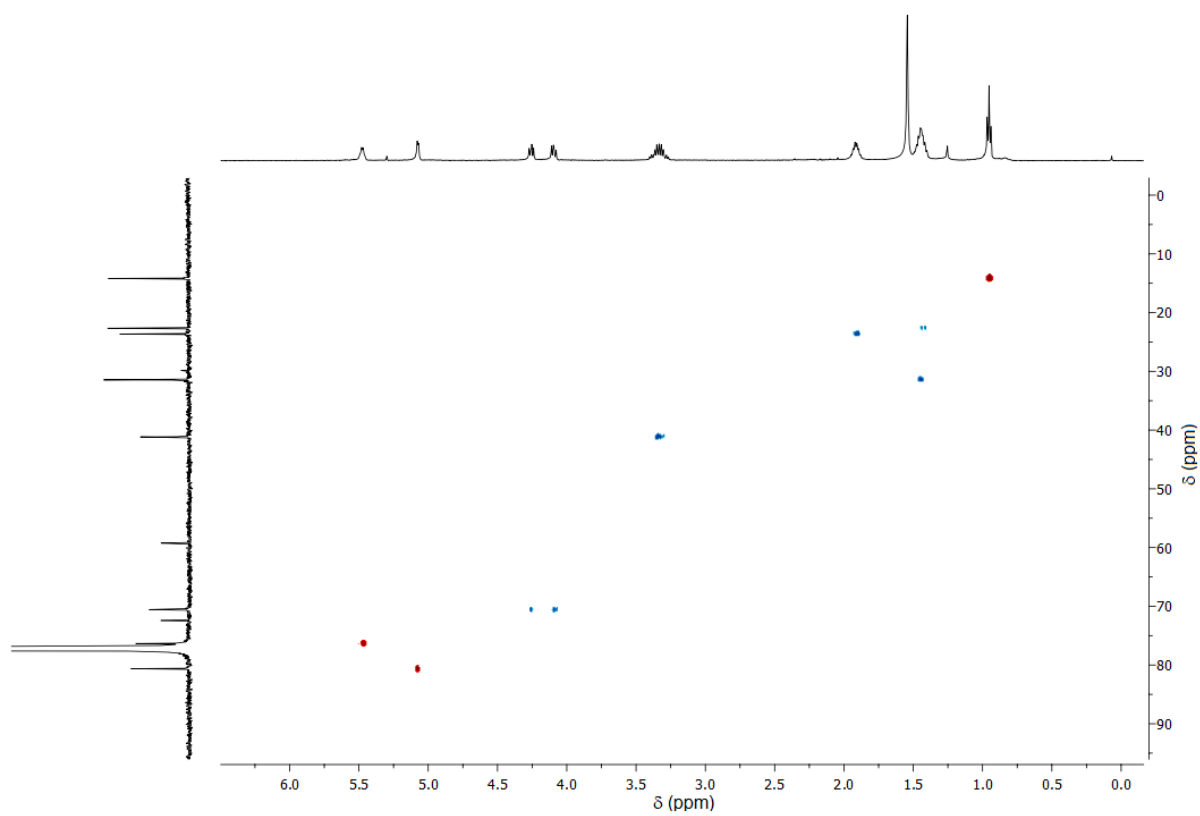
Figure S34. HSQC spectrum of **13**IM in CDCl₃.
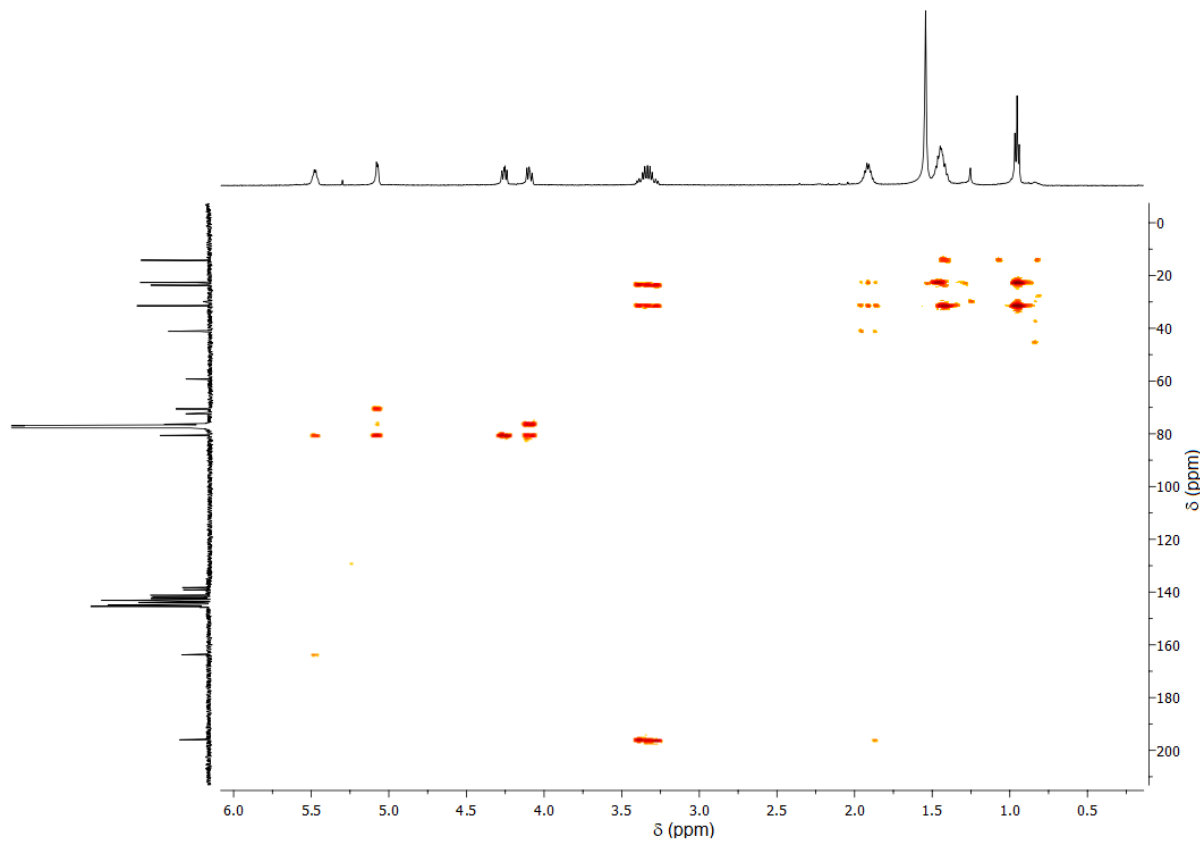
Figure S35. HMBC spectrum of **13**IM in CDCl₃.

a)
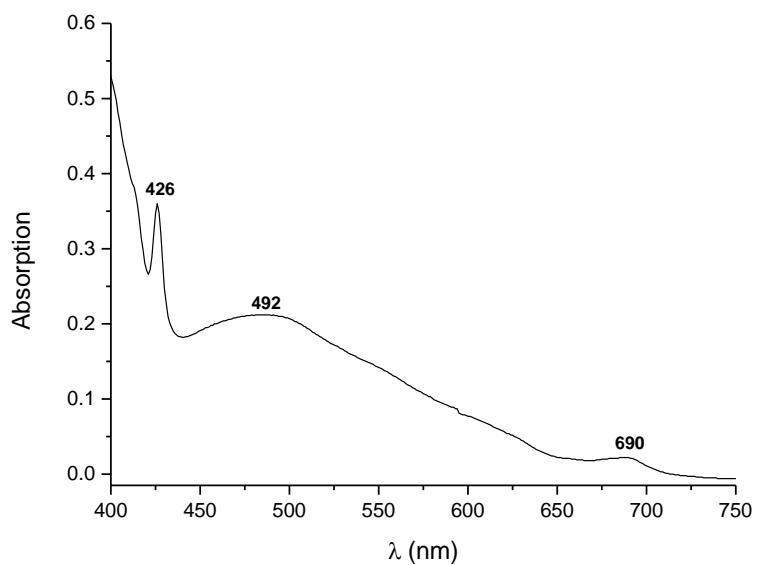
λ (nm)	ε (dm^3 mol^{-1} cm^{-1})
426	8392
492	4918
690	513

b)
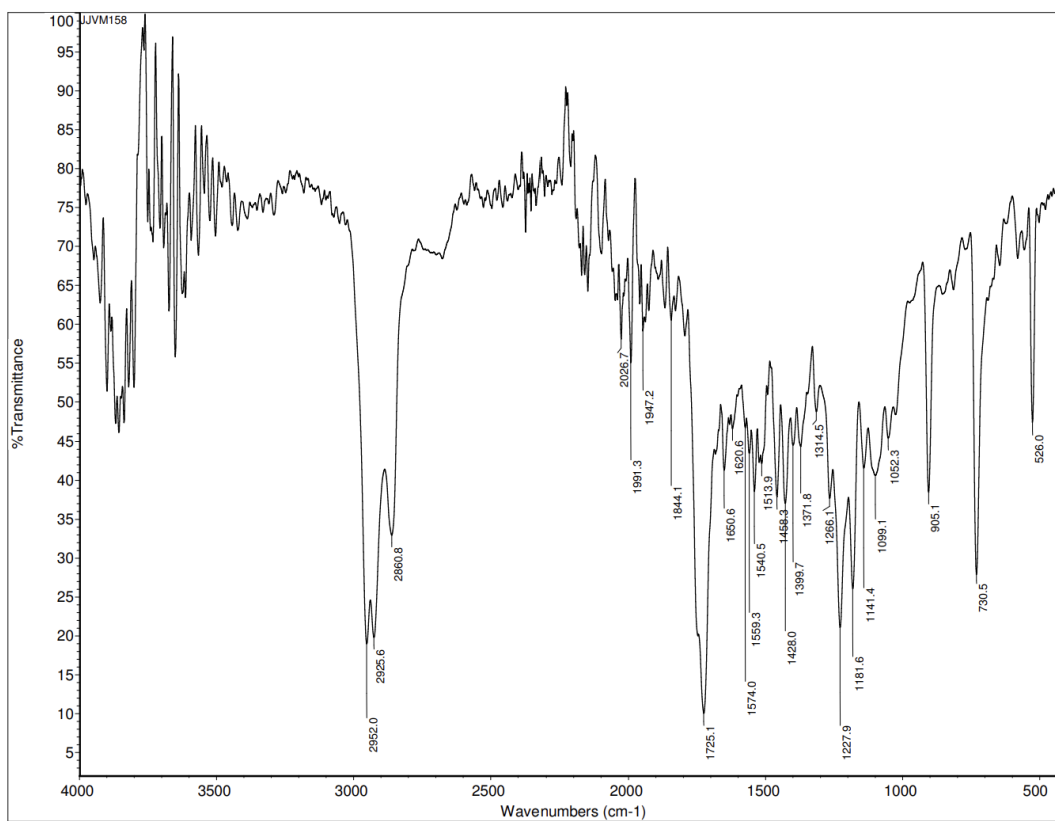
Figure S36. a) UV-vis absorption spectrum of **13$_{IM}$** compound in CHCl$_3$. b) FTIT-ATR of **13$_{IM}$**.

The solubility was determined by UV-vis spectroscopy in the following way: standard series of four different concentrations and saturated solution were prepared. For all samples the UV-vis spectra were recovered and elaborated data were presented as a graph A *vs* μ (mg/mL). Standard solutions should have absorbance in the interval 0.1-0.8 while saturated solution must be appropriately diluted to have the absorbance in the mentioned region.

Preparation of initial solution μ$_0$: 1.5 mg of **11_{IM}** was measured and transferred to a volumetric flask and dissolved by the addition of toluene to 5 mL. The absorbance of initial solution μ$_0$ was out of the mentioned region (0.1-0.8).

Preparation of standard series: The solution μ$_1$ was prepared by diluting 3.5 mL of μ$_0$ to 5 mL in volumetric flask (5 mL) and every second solution was prepared in the same way by diluting the previous solution.

Standard solution	μ (mg/mL)	A^{429nm}
1	0.2100	0.630
2	0.1470	0.393
3	0.1029	0.244
4	0.0720	0.149

Graph of concentration (mg mL^{-1}) versus absorbance:

Equation	y = a + b*x	
Weight	No Weighting	
Residual Sum of Squares	2.34321E-4	
Pearson's r	0.99911	
Adj. R-Square	0.99733	
	Value	Standard Error
B Intercept	-0.1113	0.0149
B Slope	3.49894	0.1044
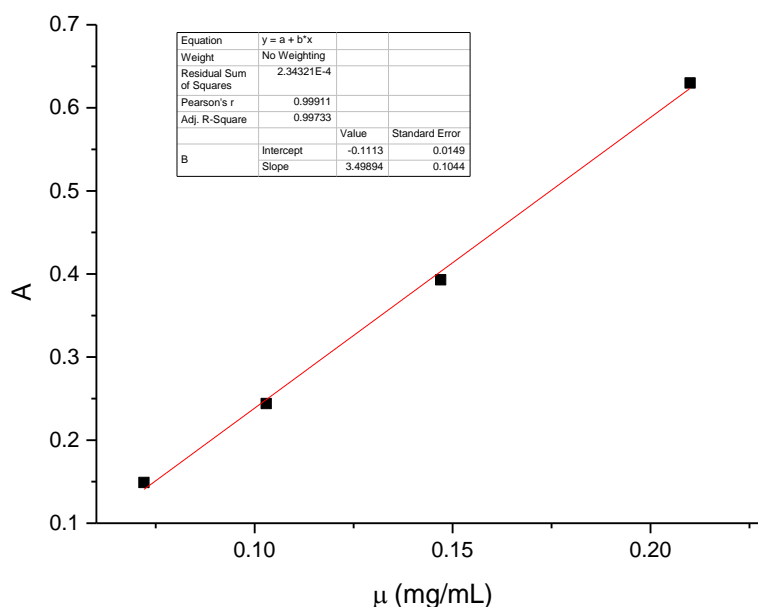
Preparation of saturated solution: saturated solution was centrifuged and supernatant was taken out and diluted. 100 μL supernatant was measured and diluted to 2 mL by addition of toluene in volumetric flask (2 mL) to get solution that has the absorbance in the mentioned region. The solution thus obtained had an absorbance of 0.378 and its mass concentration was 0.14 mg mL^{-1}.

The solubility of compound **11_{IM}** in toluene was 2.8 mg mL^{-1}.

Cyclic Voltammetry measurements
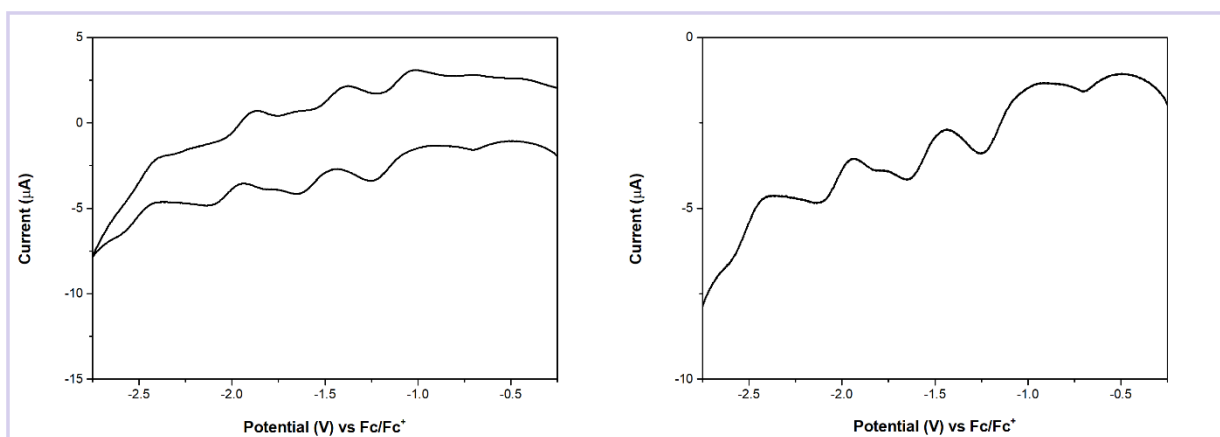
Figure S37. (left) CV, (right) Linear sweep voltammetry (LSV) of **9** (0.4 mg/mL) recorded in *o*-DCB/DMF 100/1, at 50 mVs^{-1}, at room temperature, under Argon. Potentials are shown versus Fc/Fc$^+$.
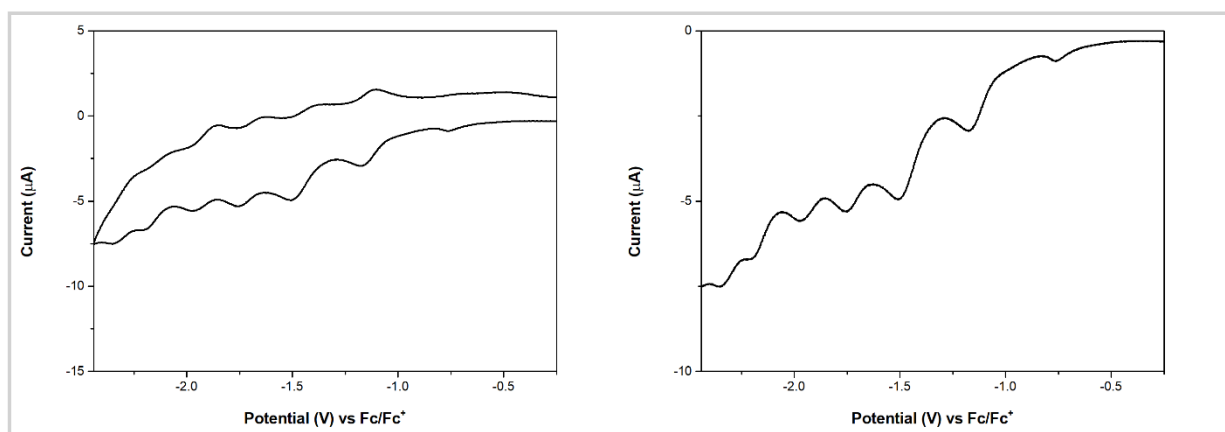
Figure S38. (left) CV, (right) Linear sweep voltammetry (LSV) of **10$_{IS}$** (0.4 mg/mL) recorded in *o*-DCB/DMF 100/1, at 50 mVs^{-1}, at room temperature, under Argon. Potentials are shown versus Fc/Fc$^+$.
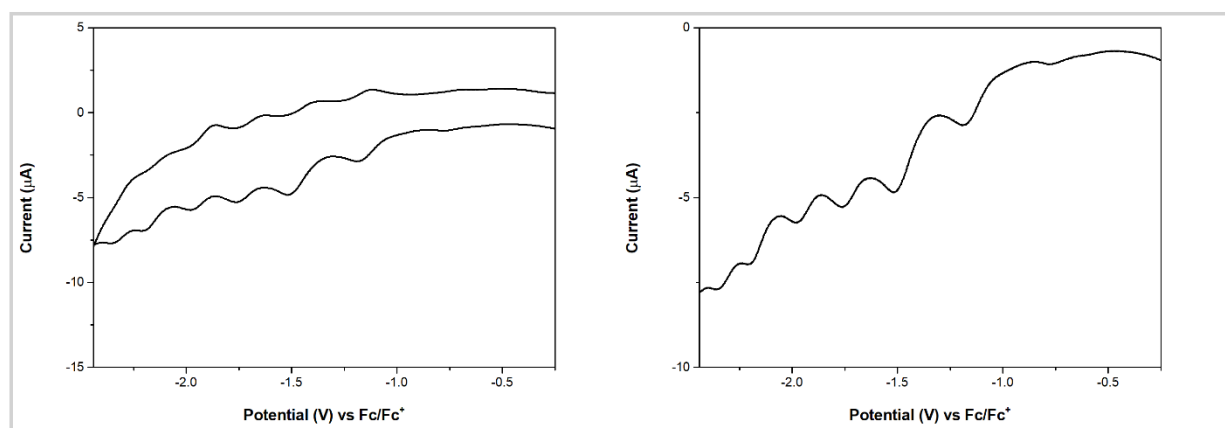
Figure 39. (left) CV, (right) Linear sweep voltammetry (LSV) of **11$_{IM}$** (0.4 mg/mL) recorded in *o*-DCB/DMF 100/1, at 50 mVs^{-1}, at room temperature, under Argon. Potentials are shown versus Fc/Fc$^+$.
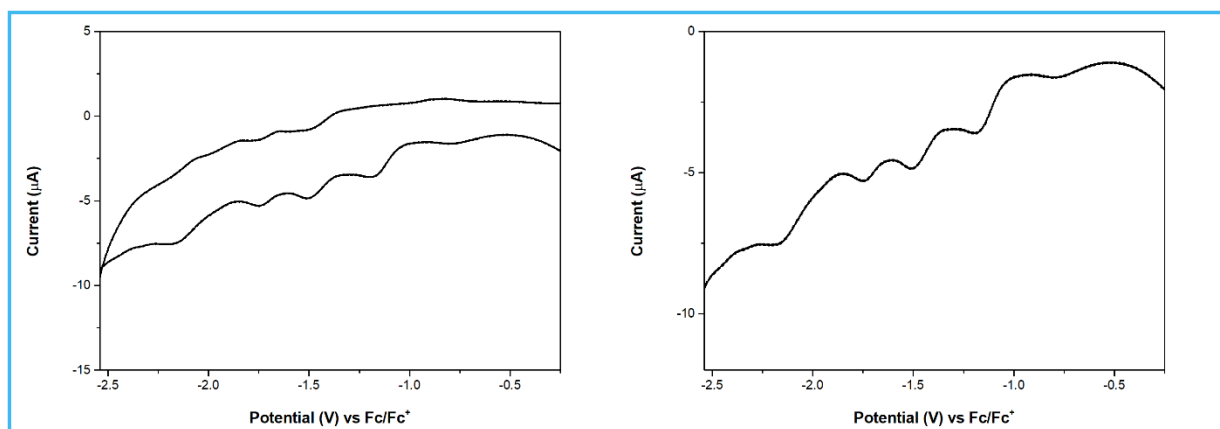
Figure S40. (left) CV, (right) Linear sweep voltammetry (LSV) of **12_{IS}** (0.4 mg/mL) recorded in *o*-DCB/DMF 100/1, at 50 mVs^{-1}, at room temperature, under Argon. Potentials are shown versus Fc/Fc$^+$.
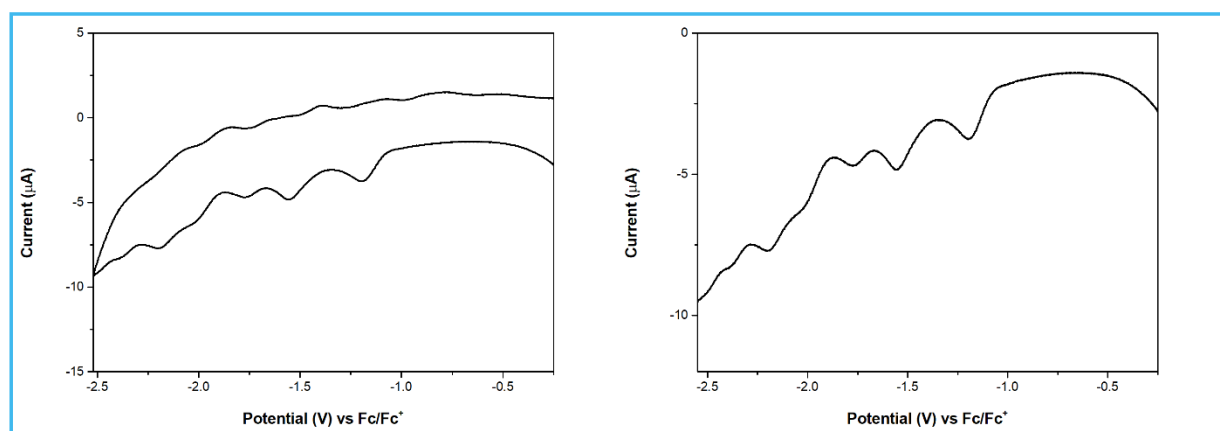
Figure S41. (left) CV, (right) Linear sweep voltammetry (LSV) of **13_{IM}** (0.4 mg/mL) recorded in *o*-DCB/DMF 100/1, at 50 mVs^{-1}, at room temperature, under Argon. Potentials are shown versus Fc/Fc$^+$.

Oxidation potential of C$_{60}$

Measured by CV; Experimental conditions: V *vs* ferrocene/ferrocenium (Fc/Fc$^+$); the reference electrode is Ag/AgCl; the working electrode is a glassy carbon electrode (GCE); 0.1 M *n*Bu$_4$NPF$_6$; scan rate: 50 mVs^{-1}; measured in *o*-DCB /
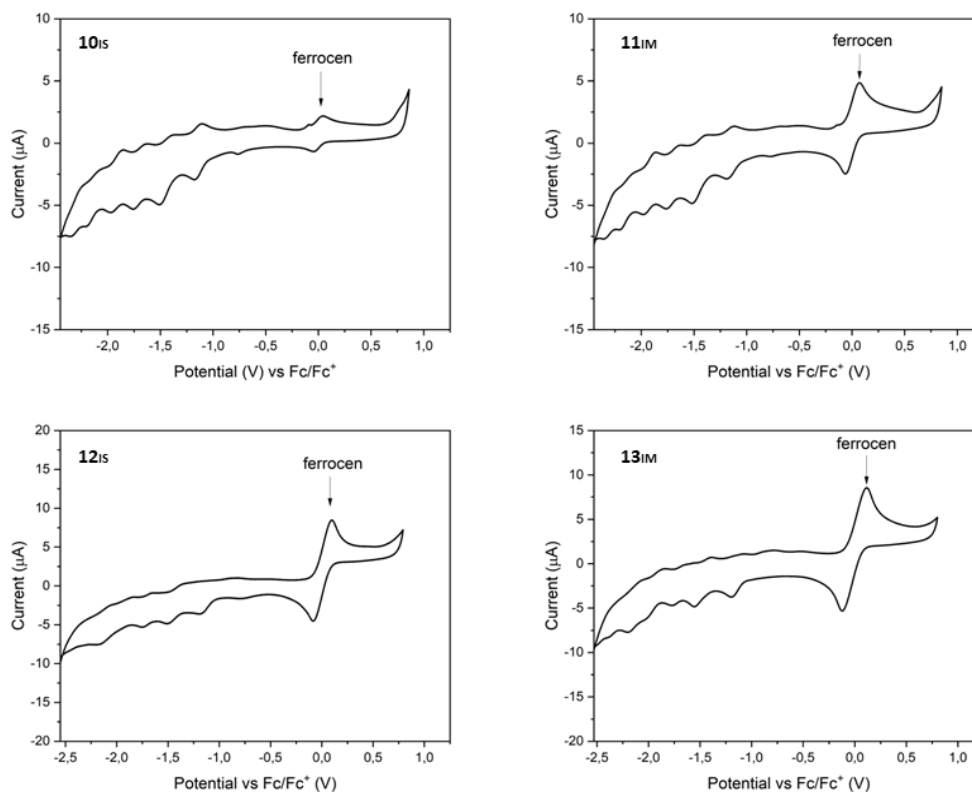
dimethylformamide (100:1 v/v) at room temperature.

Isothermal titration calorimetry (ITC):

The titration experiments were carried out using a Nano ITC-low volume calorimeter from TA Instruments. In each of the titrations, 25 injections of 0.97 μL (dumbbell → [10]CPP) or 1.95 μL ([10]CPP → dumbbell) were added from the computer-controlled 50 μL microsyringe into the corresponding solution in the measuring cell, with an interval of 200 s between the injections and a stirring rate of 350 rpm. All ITC experiments were performed at 25 °C. The respective first injections were deleted from the data sheet to eliminate the effect of titrant diffusion across the syringe tip during the equilibration process. The heat change accompanying the addition of the guest into solvent were subtracted from the raw results by the software AFFINImeter using the fitted parameter Q$_{dil}$ [cal/mol]. The concentrations used were 3.5 mM for the dumbbell molecules in the syringe and 0.035 mM for the dumbbell molecules in the sample cell. For [10]CPP there was always a concentration of 0.35 mM used in the syringe and in the sample cell. Each experiment was performed in duplicate and the experimental data were fitted to a theoretical titration curve using the software AFFINImeter with ΔH (enthalpy change in kcal mol^{-1}), K_a (association constant in M^{-1}) and n (stoichiometry), as adjustable parameters.

Thermodynamic parameters were calculated from equation (1):

$$\Delta G = \Delta H - T\Delta S = -RT \cdot lnK_a \tag{1}$$

ΔG: change in free energy; ΔH: change in enthalpy; ΔS: change in entropy; T: absolute temperature; R: universal gas constant.

Global Parameters

Par. ID	Value	STD
Qdil(1) [cal/mol]	2.0520e+2	4.4836e+0
Qdb(1) [cal]	0.0000e+0	--
rM(1)	1.0000e+0	--
rA(1)	1.0000e+0	--

Reaction Parameters

#Set	#Sites	n	STD(n)		K[M⁻ⁿ]	STD(K)		ΔH [cal/mol]	STD(ΔH)
1	n(1,1)	4.7492e-1	1.9382e-3	K$_A$ (1,1)	3.2684e+5	7.0374e+3	H$_A$ (1,1)	-1.3539e+4	6.6103e+1
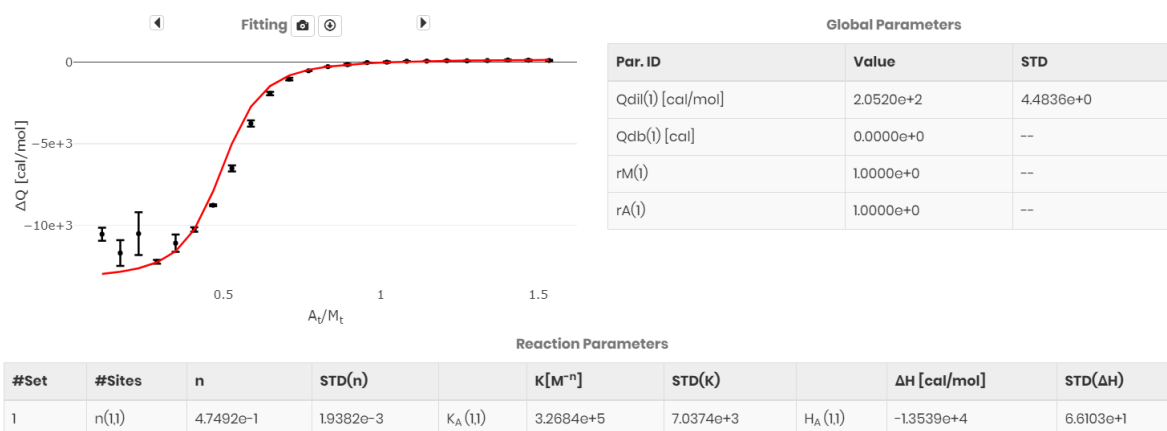
Figure S42. Analysis of the titration of **10$_{IS}$** → [10]CPP in *o*-DCB with the independent model giving n = 0.475 and showing the experimental data points (black) as well as the fitting curve (red).

Global Parameters

Par. ID	Value	STD
Qdil(2) [cal/mol]	-2.6702e+3	7.7282e+1
Qdb(2) [cal]	0.0000e+0	--
rM(2)	1.0000e+0	--
rA(2)	1.0000e+0	--

Reaction Parameters

#Set	#Sites	n	STD(n)		K[M⁻ⁿ]	STD(K)		ΔH [cal/mol]	STD(ΔH)
1	n(1,1)	1.8288e+0	1.6652e-2	K$_A$ (1,1)	2.6242e+5	5.3507e+4	H$_A$ (1,1)	-5.4166e+3	1.7919e+2
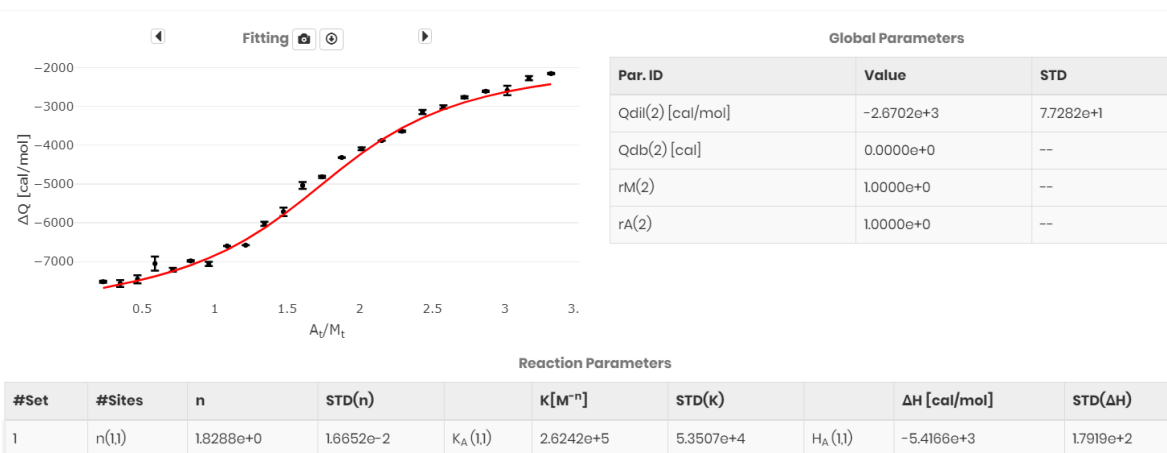
Figure S43. Analysis of the titration of [10]CPP → **10$_{IS}$** in *o*-DCB with the independent model giving n = 1.83 and showing the experimental data points (black) as well as the fitting curve (red).

Global Parameters

Par. ID	Value	STD
Qdil(1) [cal/mol]	-6.5884e+1	1.5402e+2
Qdb(1) [cal]	0.0000e+0	--
rM(1)	1.0000e+0	--
rA(1)	1.0000e+0	--

Reaction Parameters

#Set	#Sites	n	STD(n)		K[M⁻ⁿ]	STD(K)		ΔH [cal/mol]	STD(ΔH)
1	n(1,1)	4.8717e-1	2.1350e-2	K$_A$ (1,1)	2.2131e+5	5.4209e+4	H$_A$ (1,1)	-1.1878e+4	3.4287e+3
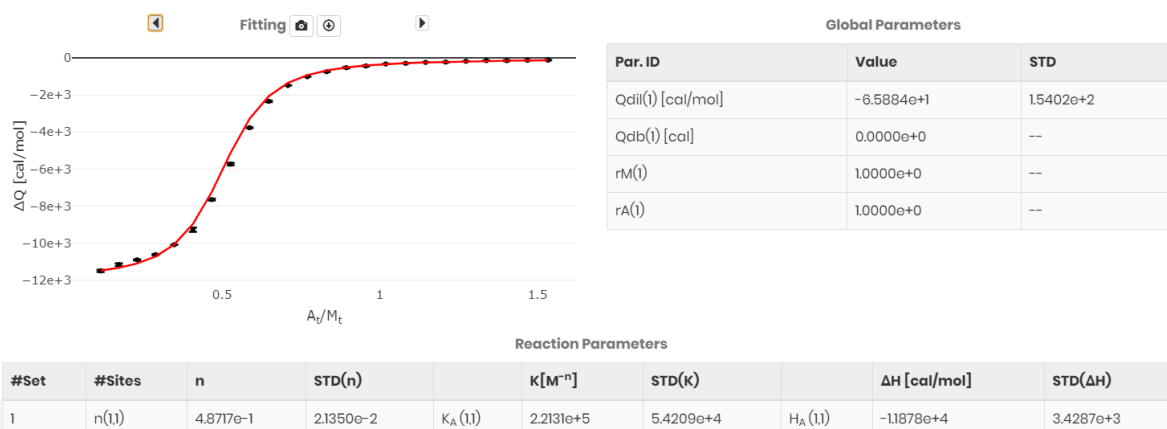
Figure S44. Analysis of the titration of **11$_{IM}$** → [10]CPP in *o*-DCB with the independent model giving n = 0.487 and showing the experimental data points (black) as well as the fitting curve (red).

Global Parameters

Par. ID	Value	STD
Qdil(1) [cal/mol]	−4.5587e+2	2.5931e+2
Qdb(1) [cal]	0.0000e+0	--
rM(1)	1.0000e+0	--
rA(1)	1.0000e+0	--

Reaction Parameters

#Set	#Sites	n	STD(n)		K[M⁻ⁿ]	STD(K)		ΔH [cal/mol]	STD(ΔH)
1	n(1,1)	2.3238e+0	7.9188e-2	K_A (1,1)	4.1413e+4	3.3199e+3	H_A (1,1)	−9.7264e+3	4.2172e+2
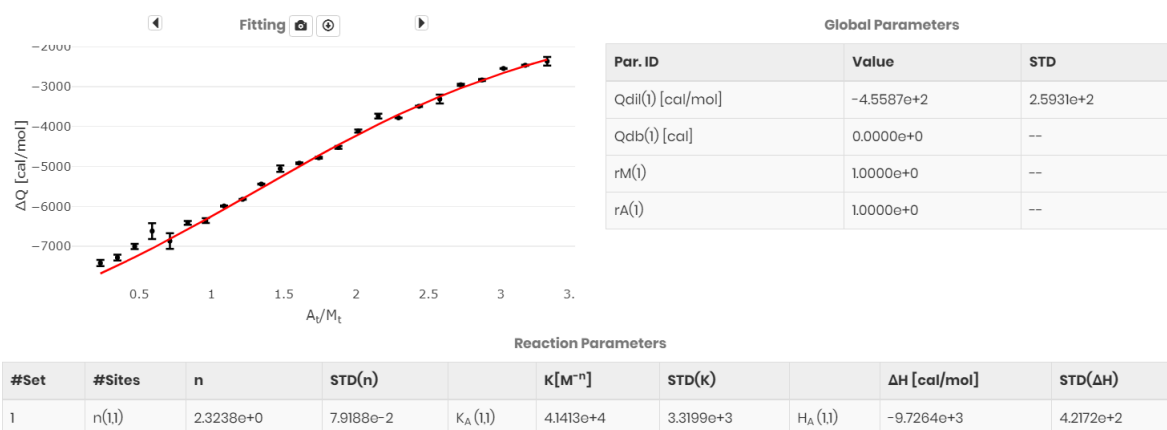
Figure S45. Analysis of the titration of **11**IM → [10]CPP in *o*-DCB with the independent model giving n = 2.32 and showing the experimental data points (black) as well as the fitting curve (red).

a)

b)

c)

d)

Reaction Parameters

#	Reaction	K_a [M⁻ⁿ]	STD(K)	ΔH [cal/mol]	STD(ΔH)
1	Free species ↔ MA	1.2783e+6	7.6761e+4	−5.2765e+3	7.4514e+1
2	+ M ↔ M₂A	1.2554e+5	1.0776e+4	−4.9162e+3	1.8836e+2
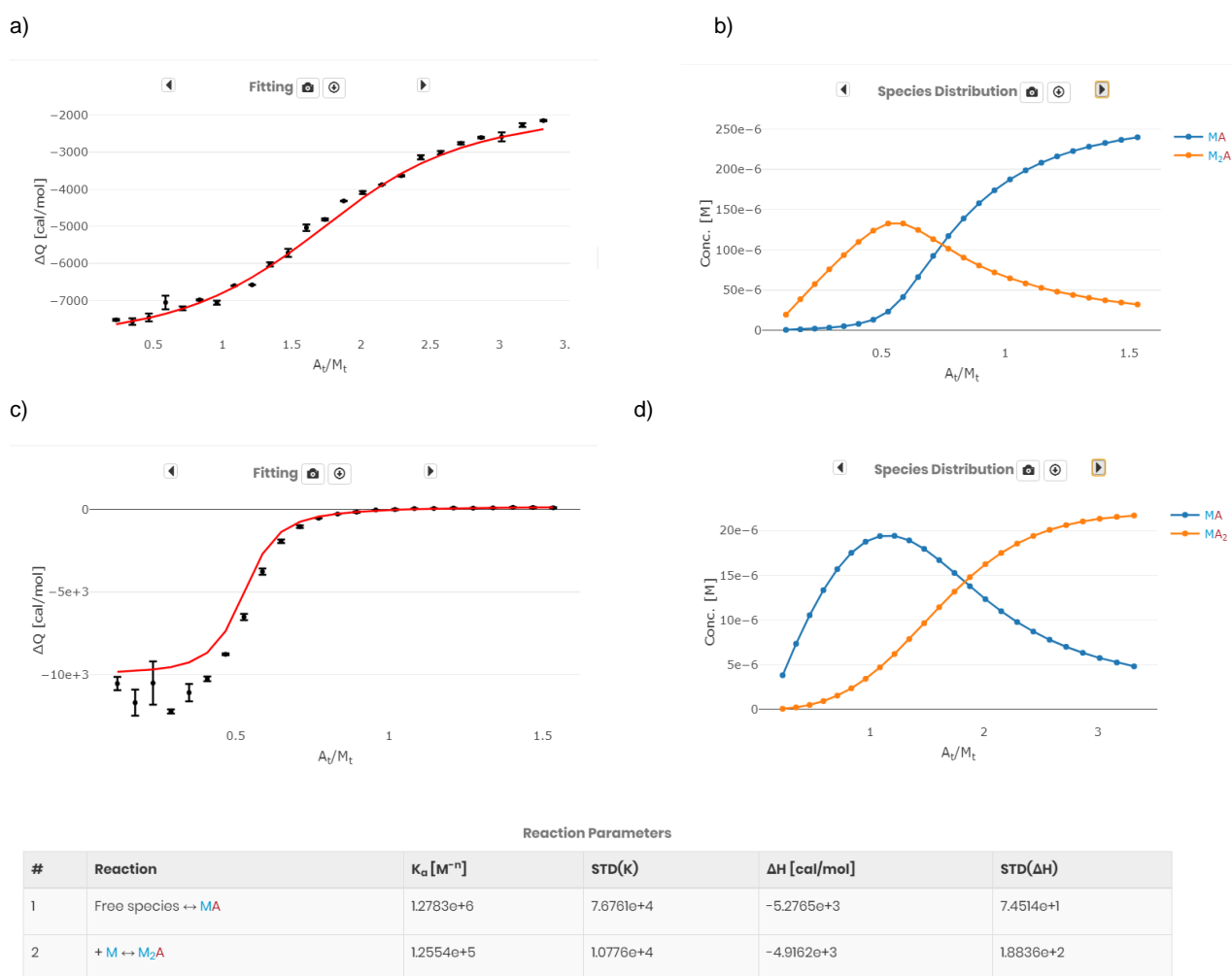
Figure S46. Global analysis of the titration of **10**IS → [10]CPP (a+b) together with [10]CPP → **10**IS (c+d) in *o*-DCB using a 1:2 (a) and 2:1 (c) binding model, showing the experimental data points (black) and the fitting curve (red) (a+c) as well as the species distribution of [10]CPP⊃**10**IS (blue) and ([10]CPP)₂⊃**10**IS (orange) during the titrations in both directions (b+d).

33

a)

b)

c)

d)
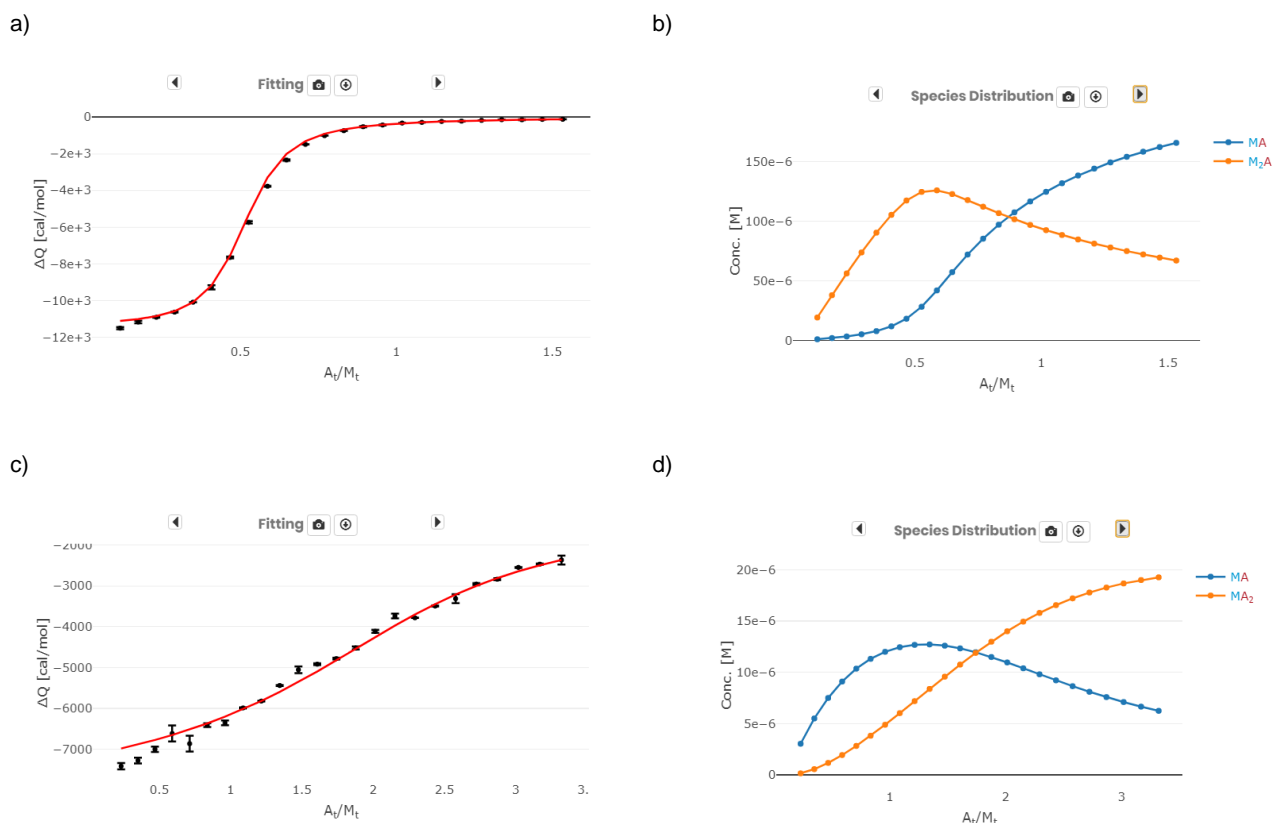
Reaction Parameters

#	Reaction	$K_a\ [M^{-n}]$	STD(K)	$\Delta H\ [cal/mol]$	STD(ΔH)
1	Free species $\leftrightarrow$ MA	1.4976e+5	1.0645e+4	−5.9523e+3	3.7059e+1
2	+ M $\leftrightarrow$ M$_2$A	7.8265e+4	5.9851e+3	−5.4585e+3	3.2558e+1

Figure S47. Global analysis of the titration of **11$_{IM}$** → [10]CPP (a+b) together with [10]CPP → **11$_{IM}$** (c+d) in *o*-DCB using a 1:2 (a) and 2:1 (c) binding model, showing the experimental data points (black) and the fitting curve (red) (a+c) as well as the species distribution of [10]CPP⊃**11$_{IM}$** (blue) and ([10]CPP)$_2$⊃**11$_{IM}$** (orange) during the titrations in both directions (b+d).

Global Parameters

Par. ID	Value	STD
Qdil(1) [cal/mol]	−5.2003e+0	6.7304e+0
Qdb(1) [cal]	0.0000e+0	--
rM(1)	1.0000e+0	--
rA(1)	1.0000e+0	--

Reaction Parameters

#Set	#Sites	n	STD(n)		K[M^{-n}]	STD(K)		$\Delta H\ [cal/mol]$	STD(ΔH)
1	n(1,1)	6.2513e-1	3.2095e-3	K_A (1,1)	2.6435e+5	6.7240e+3	H_A (1,1)	−1.0705e+4	1.2482e+2
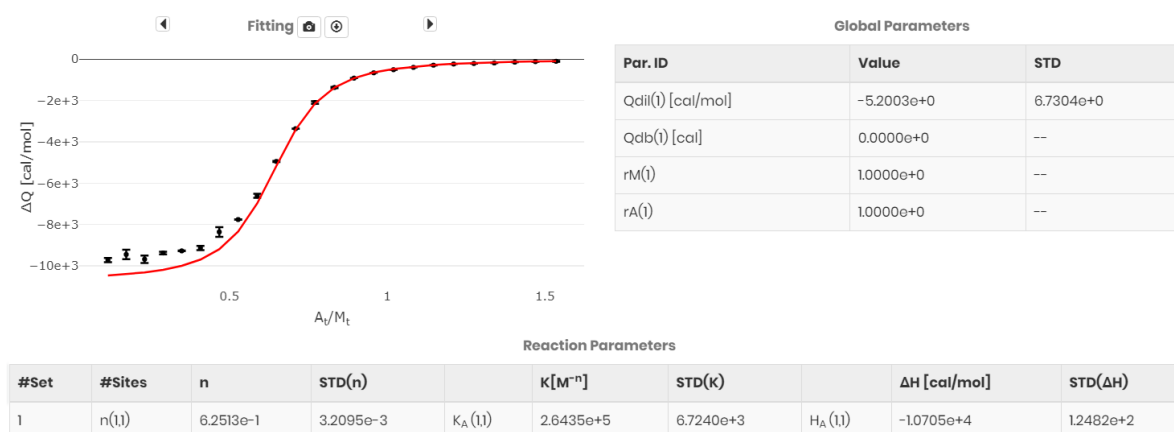
Figure S48. Analysis of the titration of **12$_{IS}$** → [10]CPP in *o*-DCB with the independent model giving n = 0.625 and showing the experimental data points (black) as well as the fitting curve (red).

Global Parameters

Par. ID	Value	STD
Qdil(1) [cal/mol]	5.4031e+1	2.2863e+1
Qdb(1) [cal]	0.0000e+0	--
rM(1)	1.0000e+0	--
rA(1)	1.0000e+0	--

Reaction Parameters

#Set	#Sites	n	STD(n)		K[M⁻ⁿ]	STD(K)		ΔH [cal/mol]	STD(ΔH)
1	n(1,1)	7.0444e-1	9.2169e-3	K$_A$ (1,1)	2.1650e+5	8.4792e+4	H$_A$ (1,1)	-9.1099e+3	2.8240e+1
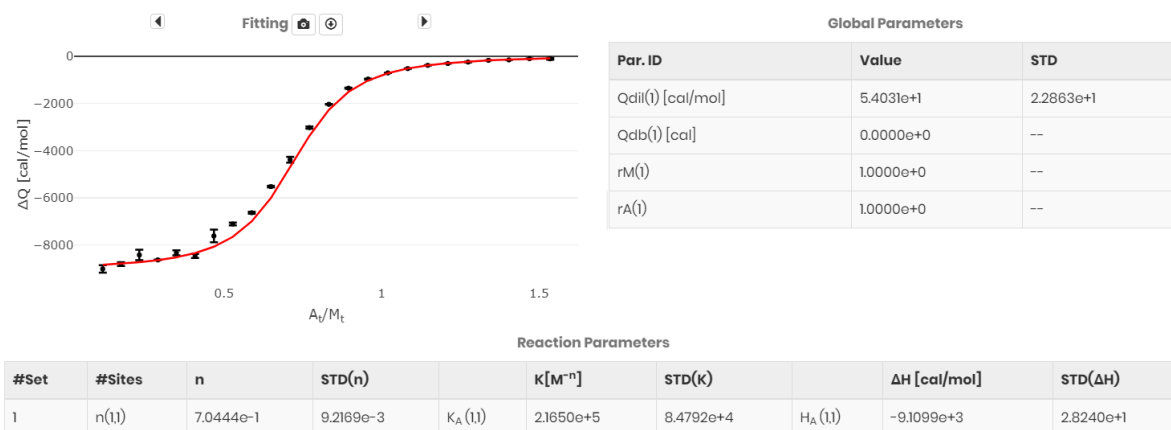
Figure S49. Analysis of the titration of **13$_{IM}$** → [10]CPP in *o*-DCB with the independent model giving n = 0.704 and showing the experimental data points (black) as well as the fitting curve (red).

Global Parameters

Par. ID	Value	STD
Qdil(1) [cal/mol]	-1.5649e+3	2.2576e+1
Qdb(1) [cal]	0.0000e+0	--
rM(1)	1.0000e+0	--
rA(1)	1.0000e+0	--

Reaction Parameters

#Set	#Sites	n	STD(n)		K[M⁻ⁿ]	STD(K)		ΔH [cal/mol]	STD(ΔH)
1	n(1,1)	1.4037e+0	6.0030e-3	K$_A$ (1,1)	3.3941e+5	1.3007e+4	H$_A$ (1,1)	-5.3792e+3	6.2758e+1
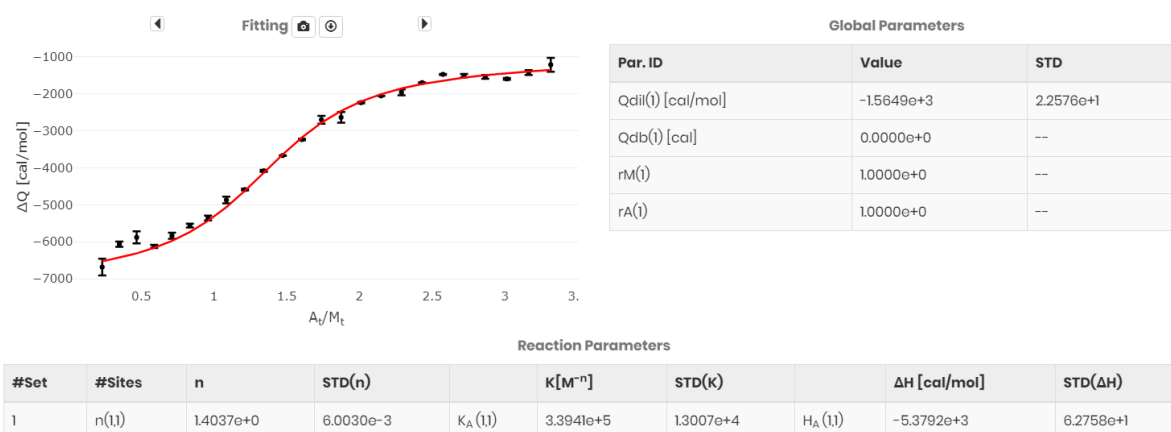
Figure S50. Analysis of the titration of [10]CPP → **12$_{IS}$** in *o*-DCB with the independent model giving n = 1.40 and showing the experimental data points (black) as well as the fitting curve (red).

Global Parameters

Par. ID	Value	STD
Qdil(1) [cal/mol]	-3.7162e+3	9.3400e+1
Qdb(1) [cal]	0.0000e+0	--
rM(1)	1.0000e+0	--
rA(1)	1.0000e+0	--

Reaction Parameters

#Set	#Sites	n	STD(n)	K[M⁻ⁿ]	STD(K)	ΔH [cal/mol]	STD(ΔH)
1	n(1,1)	1.2131e+0	2.8339e-2	K_A (1,1) 6.1945e+4	8.2355e+3	H_A (1,1) -9.6901e+3	6.7113e+2
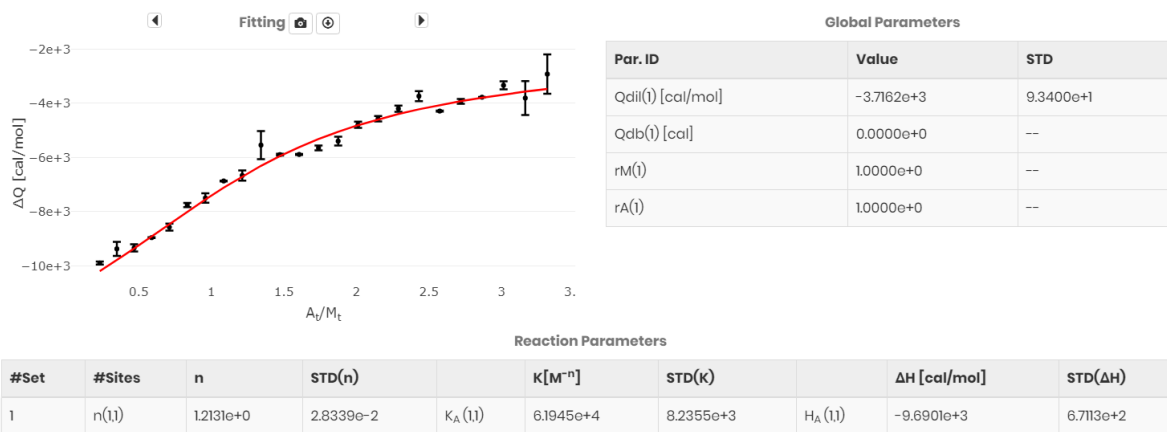
Figure S51. Analysis of the titration of [10]CPP → **13**$_{IM}$ in *o*-DCB with the independent model giving n = 1.21 and showing the experimental data points (black) as well as the fitting curve (red).

a)

b)

c)

d)

Reaction Parameters

#	Reaction	K_a [M⁻ⁿ]	STD(K)	ΔH [cal/mol]	STD(ΔH)
1	Free species ↔ MA	6.8637e+5	2.4362e+4	-8.2147e+3	1.2160e+2
2	+ M ↔ M₂A	1.5784e+4	1.0220e+3	-9.7759e+3	1.6977e+2
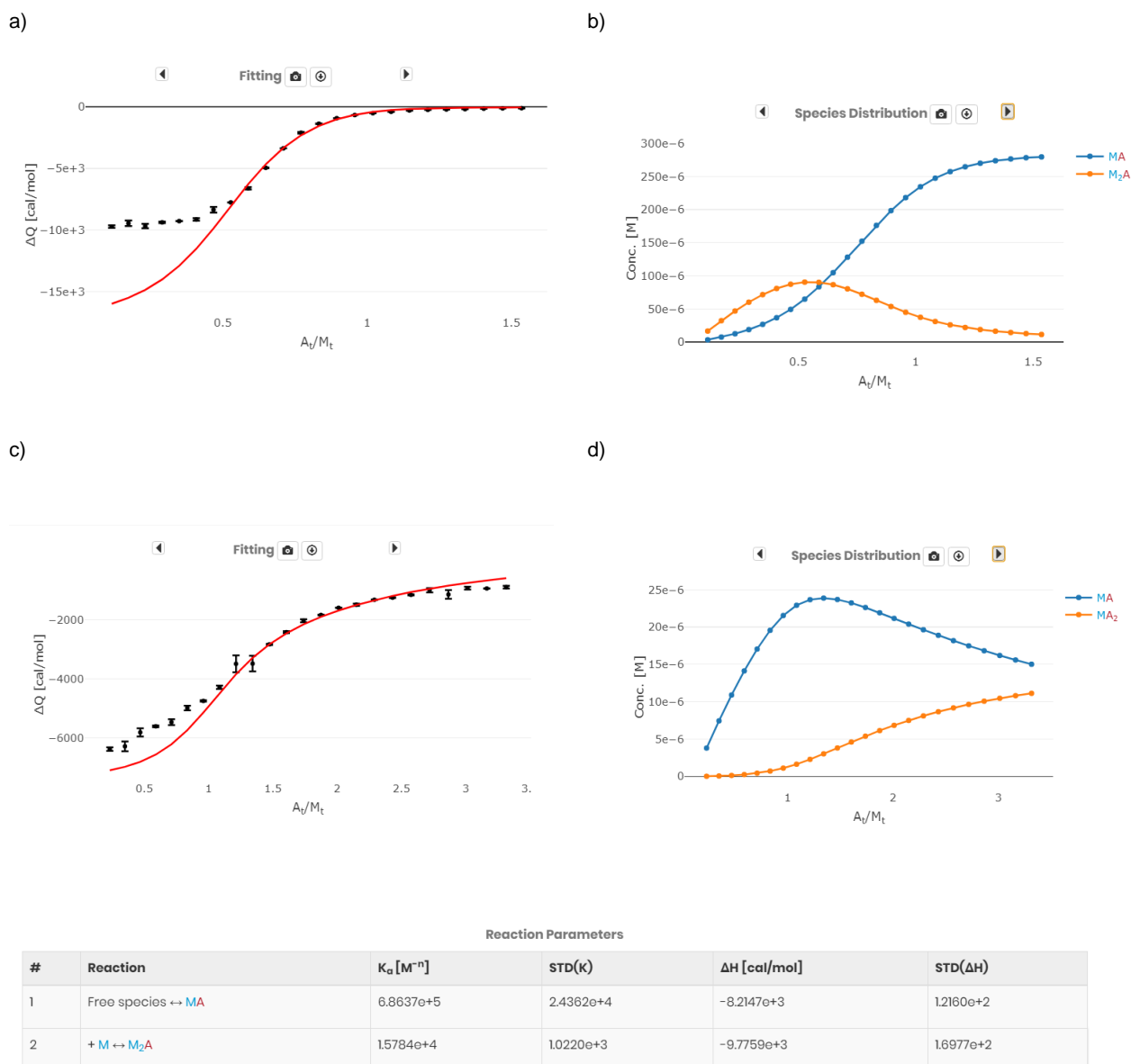
Figure S52. Global analysis of the titration of $12_{IS} \rightarrow$ [10]CPP (a+b) together with [10]CPP $\rightarrow 12_{IS}$ (c+d) in *o*-DCB using a 1:2 (a) and 2:1 (c) binding model, showing the experimental data points (black) and the fitting curve (red) (a+c) as well as the species distribution of [10]CPP⊃12_{IS} (blue) and ([10]CPP)$_2$⊃12_{IS} (orange) during the titrations in both directions (b+d).

Reaction Parameters

#	Reaction	K_a [M^{-n}]	STD(K)	ΔH [cal/mol]	STD(ΔH)
1	Free species ↔ MA	3.4723e+5	2.3697e+4	−6.6285e+3	1.0588e+2
2	+ M ↔ M$_2$A	1.7139e+4	2.2795e+3	−4.1214e+3	2.9302e+2

Figure S53. Global analysis of the titration of $13_{IM} \rightarrow$ [10]CPP together with [10]CPP $\rightarrow 13_{IM}$ in *o*-DCB using a 1:2 and 2:1binding model, the analysis belongs to Figure 2 in the main text.

NMR Titration

NMR titrations were performed by either adding a solution of [10]CPP in portions to a solution of 13_{IM} or vice versa. The corresponding concentrations of the respective o-DCB solutions are given in the subtitles of Figures S54 and S55. The corresponding NMR spectra were recorded on a BRUKER Avance 600 (^{1}H: 600 MHz) spectrometer. Chemical shifts are given in ppm, referenced to residual solvent signals and reported relative to external SiMe$_4$.
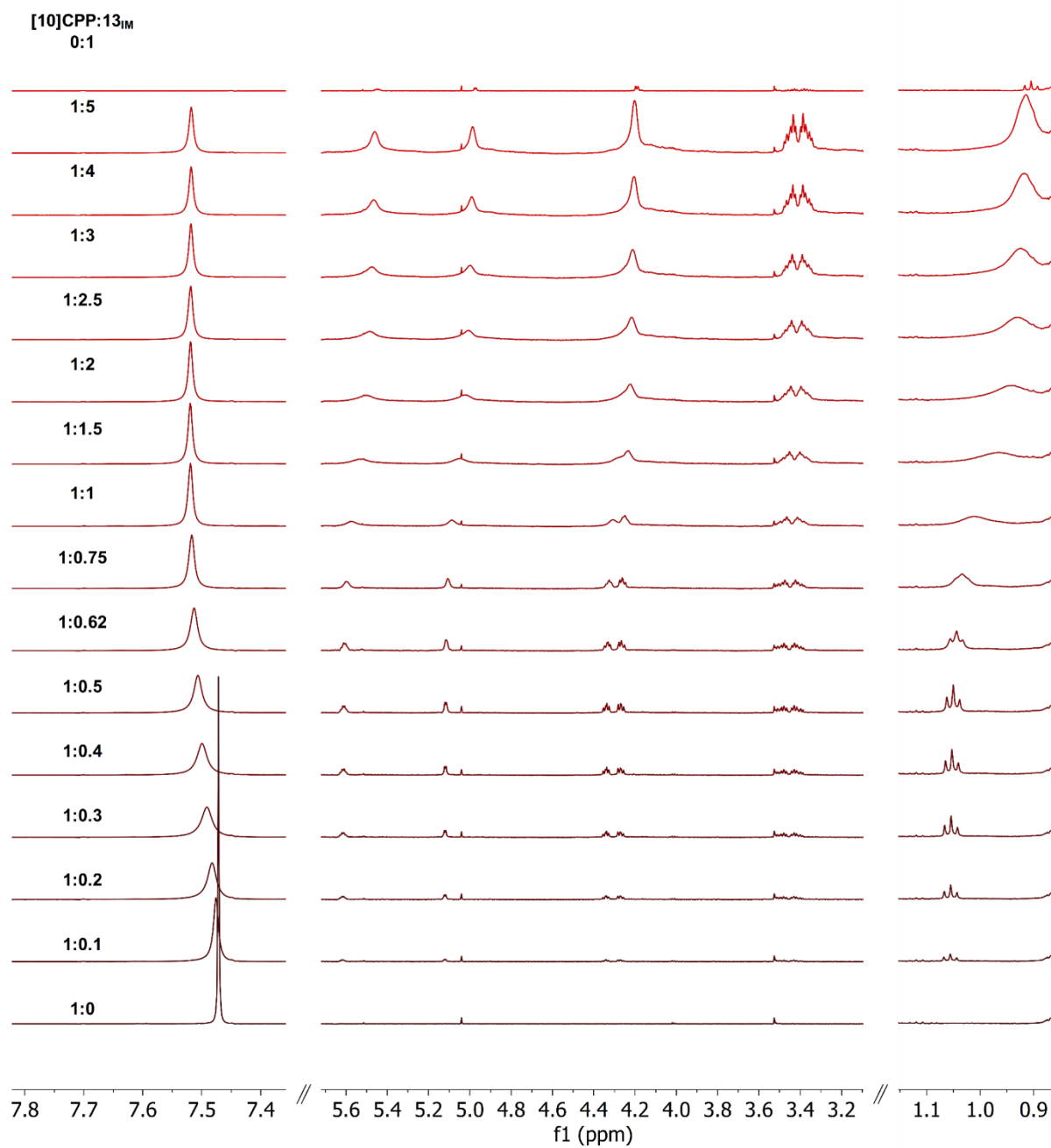
Figure S54. ^{1}H NMR (600 MHz, $C_6D_4Cl_2$, rt) spectra of the titration **13**$_{IM}$ → [10]CPP with the concentrations c(**13**$_{IM}$) = 0.00-1.17 ($\cdot$ 10^{-3} mol/L) and c([10]CPP) = 2.33-3.50 ($\cdot$ 10^{-4} mol/L) showing the shifts as well as the broadening of the [10]CPP signal (around 7.5 ppm) and the **13**$_{IM}$ signals (between 0.9-5.6 ppm).
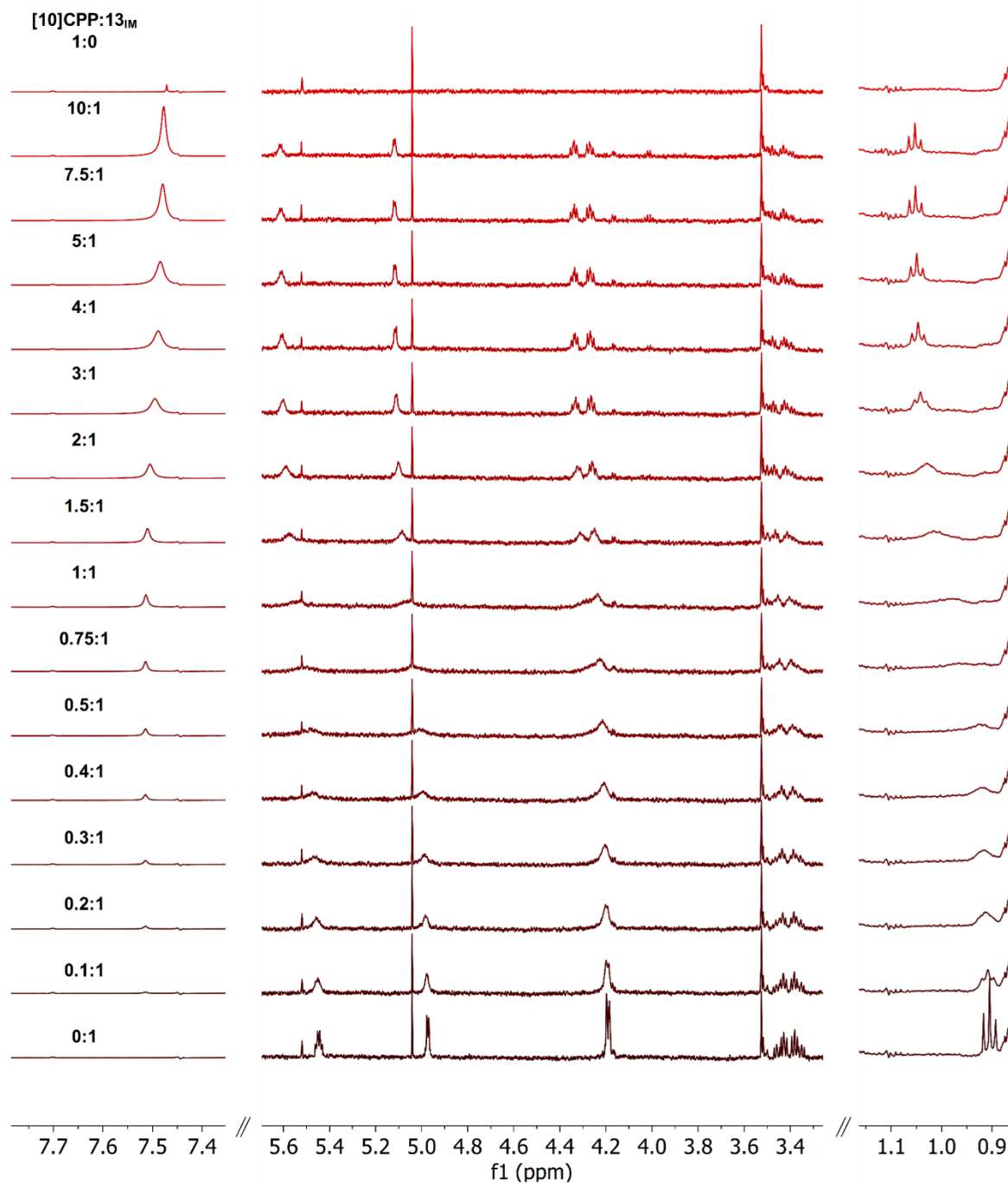
Figure S55. ^{1}H NMR (600 MHz, $C_6D_4Cl_2$, rt) spectra of the titration [10]CPP → **13**$_{IM}$ with the concentrations c([10]CPP) = 0.0-1.75 ($\cdot 10^{-4}$ mol/L) and c(**13**$_{IM}$) = 1.75-3.50 ($\cdot$ 10^{-5} mol/L) showing the shifts as well as the broadening of the [10]CPP signal (around 7.5 ppm) and the **13**$_{IM}$ signals (between 0.9-5.6 ppm).
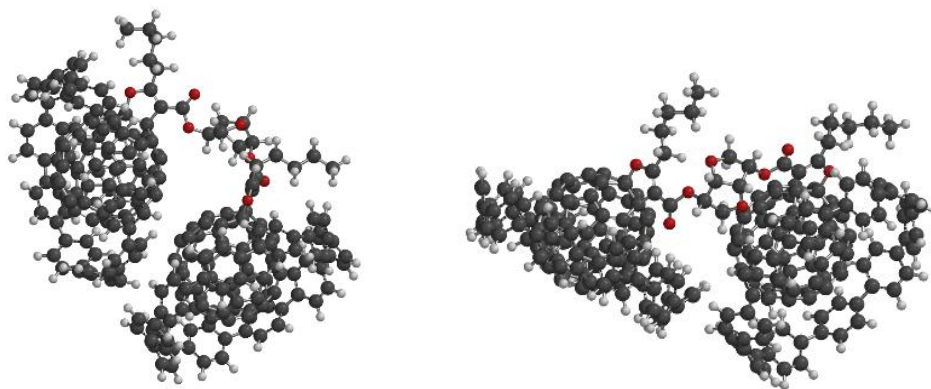
Figure S56. Structures of the 2:1 complexes ([10]CPP)$_2$⊃**10$_{IS}$** (left) and ([10]CPP)$_2$⊃**11$_{IM}$** (right) calculated with a semi-empirical method (PM6) by the Spartan'16 software.

DFT
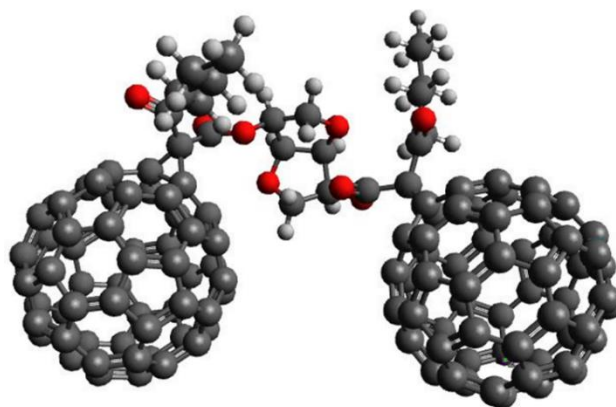
Figure S57. Optimized geometry of **11$_{IM}$** structure.
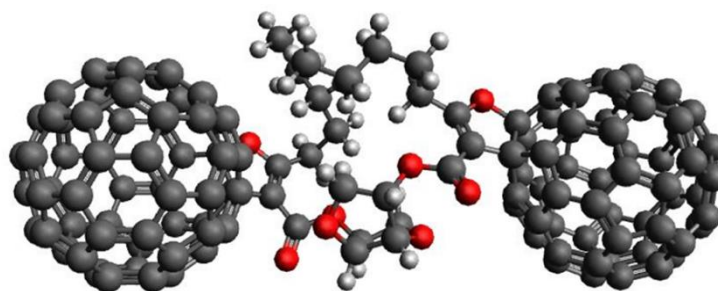
Figure S58. Optimized geometry of **13$_{IM}$** structure.

Density Functional Theory (DFT) calculations were performed using Gaussian09 software package.[23c] Geometry optimizations were performed using BLYP functional (improved with the Grimme's correction for dispersion (D3)) and 6-31G** basis set. [23d, e] Vibrational spectra were calculated to confirm that the optimized structures were true minima. Optimized geometries and calculated infrared spectra were visualized using Avogadro program.[23f]

Investigation of the thermal stability of compounds 10_{IS}-13_{IM}.
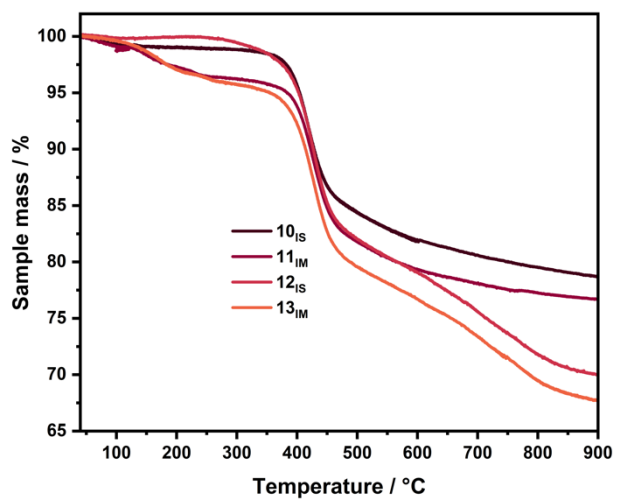
Figure S59. TGA profiles of four dumbbell molecules.